

Estimation of the correlation structure of crustal velocity heterogeneity from seismic reflection data

Marie Scholer*, James Irving* and Klaus Holliger

Institute of Geophysics, University of Lausanne, CH-1015 Lausanne, Switzerland. E-mail: james.d.irving@gmail.com

Accepted 2010 August 24. Received 2010 August 24; in original form 2009 December 3

SUMMARY

Numerous sources of evidence point to the fact that heterogeneity within the Earth's deep crystalline crust is complex and hence may be best described through stochastic rather than deterministic approaches. As seismic reflection imaging arguably offers the best means of sampling deep crustal rocks *in situ*, much interest has been expressed in using such data to characterize the stochastic nature of crustal heterogeneity. Previous work on this problem has shown that the spatial statistics of seismic reflection data are indeed related to those of the underlying heterogeneous seismic velocity distribution. As of yet, however, the nature of this relationship has remained elusive due to the fact that most of the work was either strictly empirical or based on incorrect methodological approaches. Here, we introduce a conceptual model, based on the assumption of weak scattering, that allows us to quantitatively link the second-order statistics of a 2-D seismic velocity distribution with those of the corresponding processed and depth-migrated seismic reflection image. We then perform a sensitivity study in order to investigate what information regarding the stochastic model parameters describing crustal velocity heterogeneity might potentially be recovered from the statistics of a seismic reflection image using this model. Finally, we present a Monte Carlo inversion strategy to estimate these parameters and we show examples of its application at two different source frequencies and using two different sets of prior information. Our results indicate that the inverse problem is inherently non-unique and that many different combinations of the vertical and lateral correlation lengths describing the velocity heterogeneity can yield seismic images with the same 2-D autocorrelation structure. The ratio of all of these possible combinations of vertical and lateral correlation lengths, however, remains roughly constant which indicates that, without additional prior information, the aspect ratio is the only parameter describing the stochastic seismic velocity structure that can be reliably recovered.

Key words: Inverse theory; Spatial analysis; Fractals and multifractals; Controlled source seismology; Statistical seismology; Wave scattering and diffraction.

1 INTRODUCTION

Extensive research on exposures of a variety of lower, middle and upper crystalline crustal rocks, as well as the analysis of deep borehole logs, have indicated that crustal seismic heterogeneity is often complex and hence most effectively characterized using stochastic approaches (Leary 1991; Holliger & Levander 1992; Holliger *et al.* 1993; Holliger & Levander 1994; Levander *et al.* 1994a; Wu *et al.* 1994; Goff & Levander 1996; Holliger 1996; Larkin *et al.* 1996; Holliger 1997; Dolan *et al.* 1998). Specifically, sections of crust exposed at the earth's surface are often seen to consist of a complicated distribution of lithologies having self-affine or fractal characteristics over a broad range of scales, whose structure is well described by parametric statistical models.

Controlled-source deep seismic reflection surveys represent arguably the best means of sampling the complex heterogeneity of middle and lower crustal rocks *in situ*. Forward modelling of seismic data through velocity distributions having scale-invariant characteristics results in reflected wavefields with properties that are qualitatively similar to those recorded in such deep surveys and thus serves as further evidence for a fractal heterogeneity structure in the crust (Wu & Aki 1985; Frankel & Clayton 1986; Gibson & Levander 1988; Holliger & Levander 1992; Holliger *et al.* 1993; Roth & Korn 1993; Hestholm *et al.* 1994; Holliger *et al.* 1994; Levander *et al.* 1994a,b). In contrast to the seismic response from a typical sedimentary basin, however, crustal reflection wavefields are difficult to interpret quantitatively using traditional deterministic methods. As a result, significant interest has recently been expressed in the stochastic interpretation of such data (Gibson 1991; Hurich 1996; Pullammanappallil *et al.* 1997; Line *et al.* 1998; Bean *et al.* 1999; Hurich & Kocurko 2000; Poppeliers

*Both of these authors contributed equally to this work.

& Levander 2004; Carpentier & Roy-Chowdhury 2007; Poppeliers 2007). That is, researchers have wondered whether the statistical properties of the observed ‘backscattered’ crustal seismic wavefields can be quantitatively related to the stochastic structure of the scattering medium, in particular the underlying seismic velocity distribution. Such information may provide an effective means of classifying the geology of crustal environments, for example by linking the statistical properties of velocity to the tectonic properties and history of the probed region (Pullammanappallil *et al.* 1997; Hurich & Kocurko 2000). Parameters describing crustal velocity variability may also play an important role in a range of geodynamical problems, since they tend to be linked to key physical properties such as mechanical strength and fluid content (Bean *et al.* 1999).

In previous research on the problem of relating the spatial statistics of crustal seismic reflection wavefields to those of the underlying velocity distribution, heterogeneity in the vertical and horizontal directions has generally been considered separately, with the latter being the subject of much more intensive investigation than the former. All of these studies have focused on the second-order statistical properties of the velocity field and image, which are characterized by the corresponding autocorrelation functions or, equivalently, the power spectra (e.g. Hurich & Kocurko 2000). With regard to the vertical direction, Poppeliers & Levander (2004) and Poppeliers (2007) presented a promising approach for estimating the autocorrelation model parameters describing the underlying vertical velocity variability. Their approach involves performing spiking deconvolution, thresholding and numerical integration on recorded seismic traces to yield estimates of a bimodal velocity structure, from which the vertical correlation model parameters are then computed. Tests of this method on synthetic data have been positive and suggest that it might be further developed for effective use in the field.

Conversely, attempts to estimate the horizontal stochastic characteristics of the velocity structure from seismic data have met with comparatively little success. Initial theoretical work by Gibson (1991), Holliger *et al.* (1992, 1994) and Pullammanappallil *et al.* (1997) attempted to show that the lateral second-order statistics of the primary reflectivity section (PRS), which corresponds to the convolution of the seismic reflection coefficient distribution with the source wavelet and thus to the ideal of a perfectly imaged seismic section, should be equivalent to those of the underlying velocity field for small-magnitude velocity fluctuations. In further empirical work, the parameters describing the lateral second-order statistics of velocity and zero-offset seismic data were indeed shown to be correlated (Hurich 1996; Hurich & Kocurko 2000; Carpentier & Roy-Chowdhury 2007). However, the empirical results indicate a lack of equivalence between the parameters that is not predicted by the theoretical work. Initially, this discrepancy was attributed to characteristics present in the considered reflection data, which were obtained through finite-difference modelling, that could not be accounted for with the PRS model, such as the effects of strong multiple scattering, the presence of diffractions in the case of unmigrated or improperly migrated data, and wavefront healing (Holliger *et al.* 1992; Holliger *et al.* 1994; Hurich 1996; Hurich & Kocurko 2000). However, Carpentier & Roy-Chowdhury (2007) recently made the important point that the vertical derivative operator, which acts to convert velocity to reflection coefficients and is inherently part of the PRS model, has a significant effect on the horizontal correlation structure of an image and could alone explain the empirical findings. Bean *et al.* (1999) also noted a strong dependence of the lateral correlation structure of seismic data on the bandwidth of the seis-

mic pulse. Again, the effects of the seismic pulse are included in the PRS formulation, yet this observation is not predicted by the previous theoretical work. Further examination of the existing theoretical formulations indeed indicates logical flaws. What is thus needed is a valid mathematical formulation linking the second-order statistics of a seismic reflection image with those of the underlying velocity distribution that can be used to address the corresponding inverse problem. This formulation must properly account for key aspects of the seismic reflection experiment included in the PRS model, such as vertical differentiation of velocity and wavelet convolution, and it must be able to explain the empirical findings described above.

In this paper, using many of the same assumptions employed in previous research, we attempt to address the above problem and first derive a relationship between the 2-D autocorrelation of a seismic velocity field and that of the corresponding processed and migrated, zero-offset, seismic reflection image. The relationship is valid for the case of single scattering in the subsurface and builds upon a recent methodology presented by Irving *et al.* (2009) for estimating the correlation statistics of subsurface water content from reflection ground-penetrating radar (GPR) data. Next, we perform a simple sensitivity investigation under the idealistic conditions of no noise, solely acoustic wave propagation and zero-offset data in order to examine what aspects of the second-order statistics of velocity we might hope to recover from the statistical properties of the corresponding seismic data. Finally, we present a Monte Carlo inversion strategy to estimate the parameters describing the spatial correlation structure of velocity from the autocorrelation of a seismic image and we show the results of applying this strategy to synthetic data generated at two different frequencies and assuming two different sets of prior information.

2 MODEL DERIVATION

2.1 Previous work

We begin with a short discussion of previous theoretical formulations attempting to link the correlation structure of crustal seismic reflection data with that of the P wave velocity distribution of the probed medium. All of this work assumes that the velocity field can be written as the sum of a slowly varying deterministic or background component, $v_0(x, z)$, and a superimposed component exhibiting zero-mean stochastic fluctuations, $\Delta v(x, z)$, that gives rise to the recorded reflections and whose second-order statistics we would like to estimate:

$$v(x, z) = v_0(x, z) + \Delta v(x, z). \quad (1)$$

Assuming that density is constant or, more realistically, that the magnitude of density changes is significantly smaller than that of the velocity fluctuations and thus that impedance contrasts are controlled mostly by changes in velocity, the subsurface reflection coefficient field, $r(x, z)$, can be approximately expressed as the vertical spatial derivative of the velocity perturbation field (Pullammanappallil *et al.* 1997; Poppeliers 2007):

$$r(x, z) \approx \frac{\partial}{\partial z} \Delta v(x, z). \quad (2)$$

Now, assuming (i) that single scattering of incident wave energy prevails, an assumption that is indeed inherent to most seismic processing, imaging and interpretation strategies and is often justified in crustal studies (Hurich & Smithson 1987; Holliger 1997; Line *et al.* 1998; Poppeliers 2007); (ii) that dispersion in the crustal seismic

data is minimal or has been corrected such that a constant wavelet shape can be assumed; and (iii) that mode conversions are absent or have been removed by processing; a recorded zero-offset seismic waveform, $p(x, t)$, after proper processing and migration, can be approximately expressed as a simple convolution of the subsurface reflectivity field with the input seismic wavelet, $w(t)$:

$$\begin{aligned} p(x, t) &= w(t) * r(x, t) \\ &= w(t) * \left[\frac{\partial t}{\partial z} \frac{\partial}{\partial t} \Delta v(x, t) \right], \end{aligned} \quad (3)$$

where $*$ denotes the convolution operator and t is the seismic travelttime. Here reflectivity is mapped to time using an estimate of $v_0(x, z)$, which can be obtained from CMP analysis or seismic tomography. For a constant value of v_0 , the depth derivative term in the above equation is simply given by:

$$\frac{\partial t}{\partial z} = \frac{2}{v_0}. \quad (4)$$

Eq. (3) is the PRS model for a seismic reflection section. It considers the section as a collection of 1-D, vertical incidence, primaries-only seismograms and is widely regarded as the ideal seismic image and the goal that processing hopes to achieve (Claerbout 1985; Gibson & Levander 1990; Gibson 1991). When the underlying assumptions are satisfied, the PRS has the remarkable ability to capture the key features of realistic seismic reflection data. Indeed, as we will see in the next section, finite-difference-modelled data from weakly scattering heterogeneous structures are well predicted by the PRS formulation. It is also important to note that unmigrated and non-zero-offset seismic data can be related to the PRS using the scattering curve approach (Gibson 1991).

In previous theoretical work, the PRS formulation in eq. (3) has been used in a number of ways in an attempt to relate the lateral correlation statistics of a seismic reflection image to those of the corresponding velocity perturbation field, $\Delta v(x, z)$. Holliger *et al.* (1994) and Pullammanappallil *et al.* (1997), for example, considered the lateral correlation measure of $p(x, t)$, which is defined as the normalized lateral autocorrelation of the recorded waveform:

$$c(\delta, t) = \frac{\tilde{c}(\delta, t)}{\tilde{c}(0, t)}, \quad (5)$$

where δ is the lateral lag and

$$\tilde{c}(\delta, t) = \int p(x, t) p(x + \delta, t) dx. \quad (6)$$

Gibson (1991) and Holliger *et al.* (1992), on the other hand, considered the normalized temporal Fourier transform of the 2-D autocorrelation of $p(x, t)$, which they defined as the lateral coherence:

$$\gamma(\delta, \omega) = \frac{\Phi(\delta, \omega)}{\Phi(0, \omega)}, \quad (7)$$

where

$$\Phi(\delta, \omega) = FT \left\{ \iint p(x, t) p(x + \delta, t + \tau) dt dx \right\} \quad (8)$$

with τ being the temporal lag. Finally, Pullammanappallil *et al.* (1997) considered as another measure the $k_x - t$ spectrum of $p(x, t)$, which is obtained by simply Fourier transforming over the lateral coordinate:

$$\begin{aligned} P(k_x, t) &= w(t) * R(k_x, t) \\ &= w(t) * \left[\frac{\partial t}{\partial z} \frac{\partial}{\partial t} \Delta V(k_x, t) \right]. \end{aligned} \quad (9)$$

In all of this previous work, it was either explicitly or implicitly assumed that, because the wavelet convolution and derivative in eq. (3) operate only along the time/depth coordinate, they have no effect on the lateral correlation or coherence measures and hence these measures can be equivalently described by the same measures on the underlying velocity field. In other words, the lateral correlation and coherence measures of the PRS and velocity field should be equal and thus calculating them for the former should yield reliable estimates for the latter. However, as recently demonstrated by Carpentier & Roy-Chowdhury (2007), the process of differentiating in time or depth, and indeed any filtering operation along this dimension such as convolution with the seismic pulse (Bean *et al.* 1999), actually has a profound effect on the lateral correlation structure and thus such assumptions are not justified. With regard to the $k_x - t$ spectrum, Pullammanappallil *et al.* (1997) attempted to demonstrate that the power spectrum of $P(k_x, t)$ shows the same lateral wavenumber dependence as that of $\Delta V(k_x, t)$. In doing so, however, they appear to have missed the fact that computing a power or amplitude spectrum on eq. (9) is a non-linear operation, which means that the time-domain convolution and derivative operations cannot be separated from the k_x behaviour.

To summarize, previous theoretical work has incorrectly justified the separation of vertical filtering operations from the horizontal correlation statistics of a seismic image and has suggested that the lateral statistics of velocity are simply equivalent to those of the image under the PRS approximation. What is now required is an analytically correct formulation linking the spatial correlation structure of a velocity field with that of the related seismic reflection section, that accounts for the important details discussed above and can thus be successfully used in the corresponding inverse problem.

2.2 Conceptual model

We also begin with the assumption that a properly processed and migrated zero-offset seismic reflection image can be expressed as a convolution product of the subsurface reflectivity field with the seismic wavelet. Unlike in previous theoretical formulations, however, we express the PRS model in the depth domain:

$$\begin{aligned} p(x, z) &= w(z) * r(x, z) \\ &= w(z) * \frac{\partial}{\partial z} \Delta v(x, z). \end{aligned} \quad (10)$$

Inherent to the formulation in eq. (10) is the assumption that the background velocity function, $v_0(x, z)$, does not change significantly over the subsurface region being analysed such that the wavelet in the depth domain, $w(z)$, remains approximately constant. This implies that the wavelet in depth is not stretched or compressed because of significant velocity changes. We feel that this assumption is justified as large-scale crustal velocity structure generally only exhibits relatively small variations. However, regions where wavelet shape changes significantly could be considered separately in an analysis if necessary.

As mentioned, the PRS model, either expressed in time or depth, does a good job of capturing the overall behaviour of realistic seismic data when the underlying assumptions are approximately satisfied. We have found that this is especially the case for the correlation statistics of the seismic data. However, one addition to this formulation that we have found to be necessary for its general applicability under a wide range of scenarios is accounting for the horizontal resolution limits of a migrated seismic image. It is well known that horizontal resolution in an unmigrated seismic reflection

section is limited by the Fresnel zone, which essentially describes the area on a subsurface reflector that contributes to the recorded data (e.g. Berkhout 1984). The radius of the Fresnel zone increases with depth and wavelength and hence unmigrated reflection sections have a horizontal resolution, that worsens with increasing depth and decreasing frequency. The process of migration acts to effectively collapse the size of the Fresnel zone to a uniform theoretical value on the order of the dominant wavelength and thus to improve the lateral resolution everywhere in a reflection image (Berkhout 1984; Stolt & Benson 1986). However, this lateral resolution limit is not predicted by eq. (10), as all mathematical operations occur along the vertical dimension. To accurately capture the correlation statistics of realistic seismic data under a wide range of conditions, it is thus necessary to modify the PRS formulation. We do this by adding a horizontal resolution filter, $h(x)$, to eq. (10) as follows:

$$p(x, z) = w(z) * \frac{\partial}{\partial z} \Delta v(x, z) * h(x). \quad (11)$$

Based on methodological considerations (e.g. Chen & Schuster 1999) as well as extensive empirical testing based on comparisons of finite-difference-modelled seismic data with those predicted by the PRS formulation, we have found that a simple Gaussian low-pass filter, whose width is determined by the dominant signal wavelength, is an effective choice for $h(x)$. This filter is of the form:

$$h(x) = \exp\left(-\frac{x^2}{2c^2}\right), \quad (12)$$

where c determines the filter width and is set such that the distance between the two points where the Gaussian reaches 1 per cent of its maximum amplitude is equal to the dominant wavelength. We fully acknowledge that other horizontal filter operators, possibly taking into account more of the details of the seismic experiment such as migration aperture, could be considered instead of eq. (12) for greater accuracy. Nevertheless, we have found that $h(x)$ as expressed above is quite effective for our purposes.

Noting that the derivative operator in eq. (11) can be treated as a filter whose position in the equation can be shifted to act on the wavelet, we can also express the modified PRS model in the following manner:

$$p(x, z) = \Delta v(x, z) * f(x, z), \quad (13)$$

where

$$f(x, z) = \frac{\partial}{\partial z} w(z) * h(x). \quad (14)$$

Here, we have simply lumped together all of the items acting on the velocity perturbation field (i.e. vertical derivative, seismic wavelet, horizontal resolution filter) into a single 2-D filter operator, $f(x, z)$, which provides us with a simple convolutional relationship between $\Delta v(x, z)$ and $p(x, z)$. Now taking the 2-D Fourier transform of eq. (13) and calculating the power spectrum of both sides, we have:

$$|P(k_x, k_z)|^2 = |\Delta V(k_x, k_z)|^2 |F(k_x, k_z)|^2, \quad (15)$$

where k_x and k_z are the horizontal and vertical wavenumbers, respectively. Taking the inverse Fourier transform and making use of the Wiener–Khinchine theorem linking the power spectrum and autocorrelation functions, we arrive at the final result:

$$R_{pp}(x, z) = R_{vv}(x, z) * R_{ff}(x, z). \quad (16)$$

Eq. (16) states that the 2-D spatial autocorrelation of the PRS seismic image, $R_{pp}(x, z)$, where x and z refer to the horizontal

and vertical lags, respectively, is related to the 2-D spatial autocorrelation of the velocity perturbation field, $R_{vv}(x, z)$, through 2-D convolution with the filter autocorrelation, $R_{ff}(x, z)$. This result, albeit simple, is powerful in the sense that it provides us with an effective and accurate link between the second-order spatial statistics of a velocity field and those of the corresponding seismic image. More specifically, knowing $R_{ff}(x, z)$, for which we require knowledge of either the spectral content or autocorrelation of the source wavelet, we can use the formulation in eq. (16) to estimate the parametric model parameters describing $R_{vv}(x, z)$ from $R_{pp}(x, z)$. As we will see in the next section, this formulation predicts the changes in lateral correlation behaviour resulting from vertical differentiation of the velocity field to produce reflection coefficients and convolution with the source wavelet. We will also see later that a relatively accurate estimate of $R_{ff}(x, z)$, which is required for the inversion, can actually be obtained from the vertical autocorrelation of the recorded seismic data at zero horizontal lag, $R_{pp}(0, z)$.

3 STOCHASTIC VELOCITY FIELDS AND SYNTHETIC SEISMIC DATA GENERATION

3.1 Velocity fields

In Sections 4 and 5, we explore using a number of models of crustal velocity fields whether, and how, it might be possible to employ eq. (16) for the estimation of the stochastic parameters describing velocity variability from deep seismic data. As mentioned, previous work on outcrop exposures of crustal rocks and deep borehole logs, as well as geophysical observations, have suggested that many areas of the crystalline crust can be described stochastically as scale-invariant over a broad range of scales. Most commonly, such band-limited fractal media are parameterized through their second-order statistics using the von Kármán family of autocorrelation functions, whose functional form in 2-D is given by (e.g. Goff & Jordan 1988)

$$C(r) = \frac{r^\nu K_\nu(r)}{2^{\nu-1} \Gamma(\nu)}, \quad (17)$$

where $K_\nu(r)$ is the modified Bessel function of the second kind of order $0 \leq \nu \leq 1$, Γ is the Gamma function and

$$r = \sqrt{(x^2/a_x^2) + (z^2/a_z^2)} \quad (18)$$

is the weighted radial autocorrelation lag, where a_x and a_z are the lateral and vertical correlation lengths, respectively. Eq. (17), whose properties are controlled by the parameters a_x , a_z and ν , defines a spatially anisotropic medium having axes of anisotropy aligned with the x and z directions and whose heterogeneity shows self-similar behaviour below the correlation length scales. Above the correlation length scales, the heterogeneity is spectrally white. The parameter ν controls the degree of the self-similarity in the medium and is related to the Hausdorff or fractal dimension, D , through $D = E + 1 - \nu$, where E is the Euclidean dimension. When $\nu = 0.5$, eq. (17) is equivalent to the exponential autocorrelation model commonly seen in geostatistics (e.g. Goovaerts 1997).

The 2-D Fourier power spectrum corresponding to eq. (17) is given by the following expression (e.g. Goff & Jordan 1988):

$$S(k) = \frac{4\pi \nu a_x a_z}{2^{\nu-1} \Gamma(\nu) (1 + k^2)^{\nu+1}}, \quad (19)$$

where

$$k = \sqrt{k_x^2 a_x^2 + k_z^2 a_z^2} \quad (20)$$

is the weighted radial wavenumber. Using this equation, random realizations having the specified von Kármán autocorrelation can be generated through a relatively simple procedure that involves combining the corresponding amplitude spectrum with a uniformly random phase spectrum and taking the inverse Fourier transform (Goff *et al.* 1994; Pullammanappallil *et al.* 1997; Carpentier & Roy-Chowdhury 2007). The thus generated realizations are continuously varying random fields. A number of studies, however, have suggested that middle to lower crustal rocks, as well as a number of upper crustal exposures, are better described by a modal distribution of properties, representing a limited number of dominant lithotypes (Holliger & Levander 1992; Holliger *et al.* 1993; Holliger *et al.* 1994; Levander *et al.* 1994a). Consequently, for all of the examples considered in this paper, we use bimodal von Kármán random fields having an equal proportion of the two components. The use of bimodal fields is common in work on this topic (Hurich 1996; Pullammanappallil *et al.* 1997; Carpentier & Roy-Chowdhury 2007; Poppeliers 2007). Please note, however, that all of our results and conclusions have been determined to be equally valid for the case of continuously varying random media.

To binarize the stochastic fields generated using eq. (19), Goff *et al.* (1994) describe a relatively simple procedure whereby the values in the continuous distribution are partitioned into high and low bins depending on whether they fall above or below a threshold value, respectively. For our case, where we have an equal proportion of the two components, this threshold is simply the mean of the realization. Each category is then assigned the desired velocity value. The resulting bimodal fields retain their von Kármán characteristics. However, as Goff *et al.* (1994) note, binarization decreases the effective value of ν of the continuously varying field by approximately a factor of 2 and also tends to increase the effective correlation lengths. From this point onwards, all values given for the three von Kármán model parameters, a_x , a_z and ν , will refer to those estimated from the bimodal fields and not those input into eq. (19) for the generation of the parent continuous stochastic fields. We estimate von Kármán parameter values from the 2-D autocorrelation of a generated bimodal stochastic field through a procedure that seeks to minimize the least-squares misfit between this autocorrelation and that predicted using eq. (17) (Hurich & Kocurko 2000; Carpentier & Roy-Chowdhury 2007). To denote the input values used to obtain the parent continuous fields, we use the variables a_{xc} , a_{zc} and ν_c .

Fig. 1(a) shows an example P wave velocity field that was generated using the stochastic simulation and bimodalization methodology described above. The model is 16 km long and 4 km deep and is discretized on a grid having cell dimension 16-by-16 m. The two velocities present in the model are 6000 and 6300 m s⁻¹, which yields a velocity contrast of 4.8 per cent. These velocity values are thought to be reasonably typical for much of the crystalline crust (Holliger & Levander 1992; Holliger *et al.* 1994; Levander *et al.* 1994a,b) and hence have been used in a large number of previous studies (Pullammanappallil *et al.* 1997; Carpentier & Roy-Chowdhury 2007; Poppeliers 2007). Please note that we use the same velocity contrast for all of the models considered in this paper. To generate the parent continuous field from which Fig. 1(a) was derived, we used input von Kármán model parameter values of $a_{xc} = 1300$ m, $a_{zc} = 260$ m and $\nu_c = 0.3$. After bimodalization, the 2-D autocorrelation of the field, shown in Fig. 1(b) and obtained using an algorithm based on the fast Fourier transform (e.g. Carpentier & Roy-Chowdhury 2007), was found to have best-fitting parameter values of $\nu = 0.15$, $a_x = 1544$ m and $a_z = 313$ m, which are consistent with available evidence of crustal seismic heterogene-

ity (e.g. Holliger & Levander 1992; Holliger *et al.* 1993; Holliger 1996).

3.3 Seismic data

To generate seismic reflection data corresponding to the binary velocity models investigated in this paper, we use the modelling code of Robertsson *et al.* (1994), which uses an explicit staggered-grid finite-difference scheme that is second-order accurate in time and fourth-order accurate in space to solve the viscoelastic wave equations. It is important to note, however, that, in our case, we do not exploit the full potential of this algorithm in the sense that we consider loss-free acoustic wave propagation only. Although this is a significant simplification of the real world, where both P and S waves propagate, our goal in this paper is to explore what might potentially be recovered regarding the correlation structure of a heterogeneous velocity field from seismic reflection data, using the conceptual model developed in Section 2. We thus work under idealized conditions, with the hope that the knowledge gained and methodologies presented might be used and further developed into a practical inversion approach for field data. To our knowledge, acoustic wave propagation has also been assumed in all previous work investigating the relationship between the stochastic structure of seismic data and the underlying velocity field. Another simplification that we make in this paper is the use of zero-offset, unstacked data with no added ambient noise. Again, these conditions are in no way meant to represent reality, where CMP stacking of deep crustal seismic recordings is generally necessary to enhance the often poor signal-to-noise ratio. Nevertheless, they allow us to test in a controlled setting just what information might be available in the seismic data regarding the correlation structure of the velocity field and have again been used in much previous work (Hurich 1996; Bean *et al.* 1999; Carpentier & Roy-Chowdhury 2007; Poppeliers 2007).

Fig. 1(c) shows the zero-offset seismic image corresponding to the velocity field in Fig. 1(a) after FDTD modelling, migration and amplitude scaling. To create the synthetic data, we used a Ricker source wavelet with a dominant frequency of 15 Hz and a bandwidth of two to three octaves, which is within the range of commonly used frequencies in deep crustal reflection seismology. The velocity field was assumed to lie between 4 and 8 km depth and was ‘sandwiched’ between two 4-km-thick layers having a constant velocity of 6150 m s⁻¹ (e.g. Hurich 1996). For simplicity, density was assumed everywhere constant at 2800 kg m⁻³. The quality factor, Q , was also set to a constant value of 1000. Absorbing boundaries were placed along the sides and bottom of the modelling region and a free-surface boundary condition was prescribed along the top (Robertsson *et al.* 1994). Zero-offset traces were recorded every 64 m across the model, meaning that the simulation of 251 sources was necessary. Using a time step of 0.001 s as determined by the Courant stability criterion, the modelling of all sources to a maximum recording time of 3.2 s took approximately 30 hr on a 3.16 GHz computer with 3.23 GB of RAM. The spatial discretization of 16 m in Fig. 1(a) corresponds to approximately ten times the minimum wavelength and thus is small enough to effectively avoid numerical dispersion in the generated data.

After the modelling was complete, the simulated seismic reflection data were depth migrated using the constant average background velocity of 6150 m s⁻¹, which was assumed to be known. This was done in the frequency-wavenumber domain using the algorithm of Stolt (1978). Again, assuming to have knowledge of the

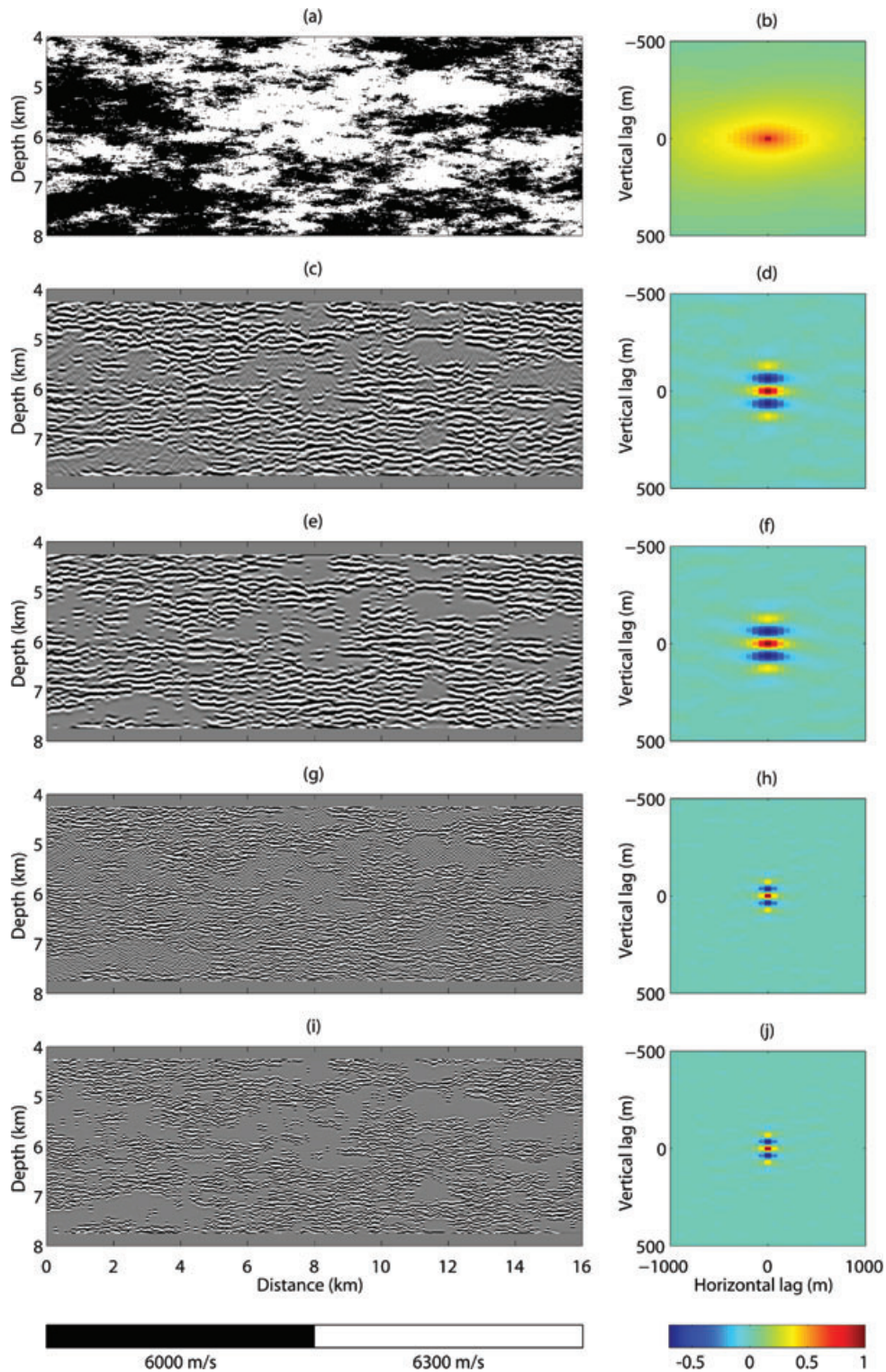


Figure 1. (a) and (b) Example bimodal velocity field and corresponding 2-D autocorrelation. (c) and (d) Migrated and gained 15 Hz zero-offset seismic reflection image, obtained by finite-difference modelling on Fig. 1(a), and corresponding autocorrelation. (e) and (f) PRS seismic image, obtained from Fig. 1(a) using eq. (11) and the same 15 Hz wavelet used for Fig. 1(c), and corresponding autocorrelation. (g) and (h) Migrated and gained 27 Hz seismic reflection image, obtained by finite-difference modelling, and corresponding autocorrelation. (i) and (j) PRS seismic image, computed using same 27 Hz wavelet, and corresponding autocorrelation.

correct background velocity for migration, and that it does not vary spatially, is quite idealistic and must be carefully considered in any field setting. The next processing step applied to the data was amplitude scaling, which was accomplished using a smooth gain function

based on the average trace envelope across the section. Note, however, that we have found the correlation statistics of the seismic reflection data, and thus the inversion methodology presented later, to be relatively insensitive to the type of gain used. Finally, the data

in Fig. 1(c) were muted between 4 and 4.25 km depth and between 7.75 and 8 km depth. This was done to suppress the horizontal reflections coming from the upper and lower bounding interfaces of the random medium, which would bias any statistical correlation analysis. The muted regions are included in Fig. 1(c) for easier comparison between the seismic image and velocity field, but they were not considered in the computation of the correlation statistics.

For comparison, Fig. 1(e) shows the synthetic seismic section computed from the velocity field in Fig. 1(a) using the modified PRS formulation in eq. (11). To create this section, we computed the reflection coefficient distribution by taking the numerical vertical derivative of the velocity field and then convolved this result with the same 15 Hz input wavelet and the horizontal resolution filter. Note how the PRS formulation does a good job of predicting the behaviour of the more realistic finite-difference-modelled seismic data, which include the effects of 2-D wave propagation and a small amount of multiple scattering. The two images look similar with regard to the location of reflecting interfaces in the subsurface and, most importantly, in terms of their overall statistical characteristics. This latter point is more clearly seen in Figs 1(d) and (f), which show the corresponding 2-D autocorrelations of the finite-difference and PRS data, respectively. The autocorrelations are almost identical and thus we see that the PRS formulation is able to capture enough of the physics of the seismic experiment to properly represent the second-order statistics of the seismic image. Also important is the distinct difference between the autocorrelations in Figs 1(d) and (f) and that of the underlying velocity model in Fig. 1(b). In going from velocity to the corresponding reflection image, we have a marked change in the 2-D autocorrelation in both the lateral and vertical directions. This is mostly caused by the simple operations of differentiation and convolution with the source pulse, which operate only along the vertical dimension. As mentioned previously, such operations cannot be separated with regard to their effect on lateral stochastic structure (Carpentier & Roy-Chowdhury 2007).

Finally, Figs 1(g) and (i) show the finite-difference and PRS-based seismic images corresponding to Fig. 1(a), obtained in an identical manner as described above, but this time using a Ricker wavelet source with a centre frequency of 27 Hz. The corresponding 2-D autocorrelations are shown in Figs 1(h) and (j). Note again how well the PRS model manages to capture the essential features of the more realistic finite-difference-based image, most importantly its stochastic structure. Also note how, as in the 15 Hz case, we have a marked difference in the autocorrelation behaviour between these images and the underlying velocity model. In comparison

with Figs 1(d) and (f), however, the correlation structure in both the vertical and horizontal directions is significantly shorter for the 27 Hz images. In the vertical direction, the reason for this is quite clear as the vertical autocorrelation behaviour is controlled directly by the spectral content of the source pulse. This is discussed in more detail below. In the horizontal direction, the reason for the difference is more complex and related to the fact that reflectors that are seen as laterally discontinuous in a higher frequency image will effectively join together and appear continuous when imaged at lower frequencies, thus increasing the apparent lateral correlation length.

4 SENSITIVITY STUDY

In Section 5, we will show how the autocorrelation of the finite-difference-modelled data in Figs 1(d) and (h) can be inverted using a Monte Carlo strategy, based on the relationship in eq. (16), to obtain information regarding the correlation structure of the velocity field in Fig. 1(a). Before going straight to the inversion, however, we first briefly investigate, through a series of carefully chosen examples, just what we might expect the second-order spatial statistics of a seismic image to reveal about the von Kármán parameters describing the stochastic structure of the underlying velocity field, under the best possible conditions. We do this in the context of a simple sensitivity study, where we examine the effect of changes in a_x , a_z and ν on the velocity field and corresponding seismic image. Although we consider below only a small number of example cases at a single frequency of 15 Hz, please note that extensive testing on a wide range of realistic synthetic data sets at different frequencies leads us to conclude that our results have general validity.

4.1 Vertical direction

To begin, we consider what, if any, information regarding the stochastic structure of velocity might remain in the vertical second-order statistics of a seismic reflection image, in our case the vertical autocorrelation $R_{dd}(0, z)$. Figs 2(a) and (b) show the vertical autocorrelation of the finite-difference-modelled seismic data from Fig. 1, along with the autocorrelation of the input seismic wavelet, for the 15 and 27 Hz cases, respectively. The results are largely identical and hence our observations suggest that $R_{dd}(0, z) \approx R_{ww}(z)$. This indicates not only a lack of sensitivity of the vertical second-order statistics of a seismic image to those of the underlying velocity

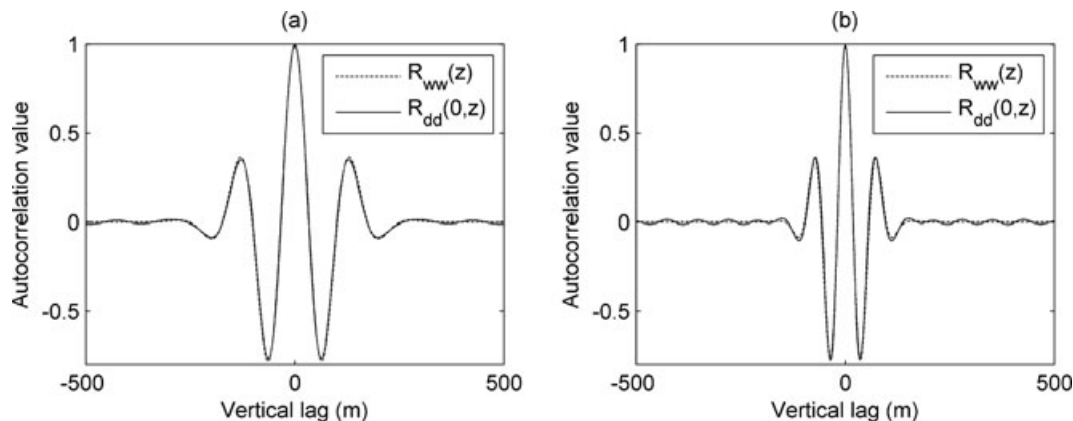


Figure 2. (a) Autocorrelation of the 15 Hz input wavelet used to create the FDTD data in Fig. 1(c) and vertical autocorrelation of the FDTD data. (b) Autocorrelation of the 27 Hz input wavelet used to create the FDTD data in Fig. 1(g) and vertical autocorrelation of the finite-difference modelled data.

field, but also that the autocorrelation of the seismic wavelet, which is required for the calculation of $R_{ff}(x, z)$ in eq. (16), can be effectively obtained from the vertical autocorrelation of the data. The reason for this result is that the power spectrum of the vertical reflection coefficient distribution for a band-limited scale-invariant seismic velocity structure is given by $-k_z^2 S(0, k_z)$ (see eq. 18), and hence for the typical case of ν -values close to zero, scales approximately as k_z^2 for $k_z a_z < 1$ and k_z for $k_z a_z > 1$. It can be shown that the corresponding autocorrelation function differs very little, indeed only in terms of its first zero-crossing, from the Dirac impulse characterizing the vertical autocorrelation of the notorious ‘white noise’ reflection coefficient model (Ulrych 1999). The methodological foundations of stochastic deconvolution, which are based on the assumption that the vertical distribution of the reflection coefficients is entirely uncorrelated or ‘white’, then tell us that, in the absence of multiples, mode conversions and dispersion, the vertical autocorrelation of corresponding seismic data is essentially equivalent to the autocorrelation of the seismic source wavelet (Yilmaz 1987). It is important to restate that Poppeliers & Levander (2004) and Poppeliers (2007) presented a relatively promising approach for estimating the vertical von Kármán parameters from seismic data. These results are not in contradiction with those presented in Fig. 2, as in their case more than just the vertical second-order statistics were considered. Specifically, both the amplitude and phase information in each trace were used to perform spiking deconvolution on the data, the results of which were then thresholded and integrated to obtain a binary velocity model that was used to estimate the vertical correlation model parameters.

4.2 Horizontal direction

We next examine how changes in a_x , a_z and ν impact the lateral correlation structure of a seismic image. We first consider the effect of changing a_x . Figs 3(a), (c), (e) show three examples of velocity fields generated using different values for a_x , while holding a_z and ν approximately constant. Figs 3(b), (d), (f) on the other hand, show the corresponding finite-difference-modelled 15 Hz seismic reflection images, which were generated in an identical manner as in Fig. 1. For all of the figures in this section, Table 1 summarizes the input von Kármán autocorrelation parameters used to create the continuous parent random fields, along with the least-squares best-fitting parameters obtained for the bimodal fields shown. In all cases, variables were held constant in terms of the input von Kármán parameters, which means that for the bimodal fields there

Table 1. List of input von Kármán parameters for the continuous ‘parent’ fields from which the velocity fields in Figs 3–6 were derived, and the corresponding best-fitting parameters for the bimodal fields. The subscript ‘c’ refers to the continuous fields.

Figure	a_{zc}	a_{xc}	ν_c	a_z	a_x	ν
3a	260	260	0.30	298	303	0.16
3c	260	1040	0.30	313	945	0.15
3e	260	1820	0.30	311	2132	0.15
4a	64	320	0.30	74	366	0.16
4c	192	960	0.30	210	1071	0.16
4e	320	1600	0.30	299	1586	0.16
5a	32	1280	0.30	36	1428	0.16
5c	128	1280	0.30	144	1436	0.16
5e	320	1280	0.30	393	1567	0.15
6a	260	1300	0.10	296	1500	0.06
6c	260	1300	0.30	313	1544	0.15
6e	260	1300	0.80	333	1724	0.47

are slight variations in the best-fitting parameters. However, we do not feel that these variations are significant enough to affect our conclusions.

Figs 3(g) and (h) show the lateral autocorrelations calculated for the velocity fields and seismic data in Figs 3(a)–(f), respectively [i.e. $R_{vv}(x, 0)$ and $R_{dd}(x, 0)$]. Figs 3(i) and (j) show the corresponding vertical autocorrelations [i.e. $R_{vv}(0, z)$ and $R_{dd}(0, z)$]. Again, the muted regions between 4 and 4.25 km depth and 7.75 and 8 km depth in the seismic images were not considered in the computation of the autocorrelations. As could be expected, we see that increasing the lateral correlation length of the velocity field indeed causes a corresponding increase in the lateral correlation length of the seismic images and thus the seismic data appear to be sensitive to this parameter, at least in the case where a_z and ν are held constant. Looking at the vertical autocorrelations, we observe that there is essentially no change in either $R_{vv}(0, z)$ or $R_{dd}(0, z)$ for the three examples. This makes sense as the input a_z was held constant and the discussion and results above do not predict the vertical correlation structure to be sensitive to anything but the seismic wavelet.

To investigate the results in Fig. 3 further, we explore in Fig. 4 the effect of increasing not only the horizontal correlation length, but also the vertical correlation length, such that the aspect ratio of the velocity heterogeneity, a_x/a_z , remains approximately constant at a value of about 5. Again, ν was held fixed for these simulations. In Figs 4(a), (c), (e) we observe a large change in the visual appearance of the velocity fields as the correlation lengths are both increased. The horizontal and vertical autocorrelations of the fields, shown in Figs 4(g) and (i), respectively, demonstrate that a_x and a_z both change significantly. In Figs 4(b), (d), (f) we see the effect of these changes on the seismic data. Just like the velocity fields, as the lateral and vertical correlation lengths increase, the seismic images become ‘simpler’ and have a less chaotic reflection structure. In Figs 4(h) and (j), however, note that we have almost no corresponding change in the horizontal or vertical seismic image autocorrelations. In the vertical case, this again makes sense as the vertical correlation structure of the image is only truly sensitive to the seismic wavelet. In the horizontal direction, the result is quite surprising and we feel important for any work in this domain of research: It suggests, as will be seen more clearly later, that stochastic velocity fields having different lateral and vertical correlation lengths, but the same aspect ratio, will generate seismic data that appear visually different, but have approximately the same horizontal correlation structure. This has significant implications for what can be recovered regarding a_x and a_z from the second-order statistics of a seismic reflection image. Specifically, it suggests that, in order to recover the horizontal correlation length of the velocity heterogeneity, we require adequate knowledge of a_z . Otherwise the inverse problem will be non-unique and there will exist many a_x – a_z combinations that will allow for an acceptable fit to the 2-D autocorrelation of the seismic image.

To investigate the above finding even further, we examine in Fig. 5 the effect on the seismic image and its autocorrelation structure of varying a_z , while holding a_x and ν approximately constant. Again, we observe in Figs 5(a)–(f) a significant change in both the velocity fields and their corresponding seismic images when only a_z is increased, in the sense that both can be seen to depart from a predominantly horizontally layered structure. In Figs 5(g) and (i), we confirm that the horizontal autocorrelation structure of velocity does not change, whereas the vertical structure indeed changes significantly. Fig. 5(j) shows again that the vertical correlation structure of the seismic image is not affected by these changes, as it depends solely on the input seismic wavelet. In Fig. 5(h), however, we see a large change in the horizontal correlation structure of the seismic

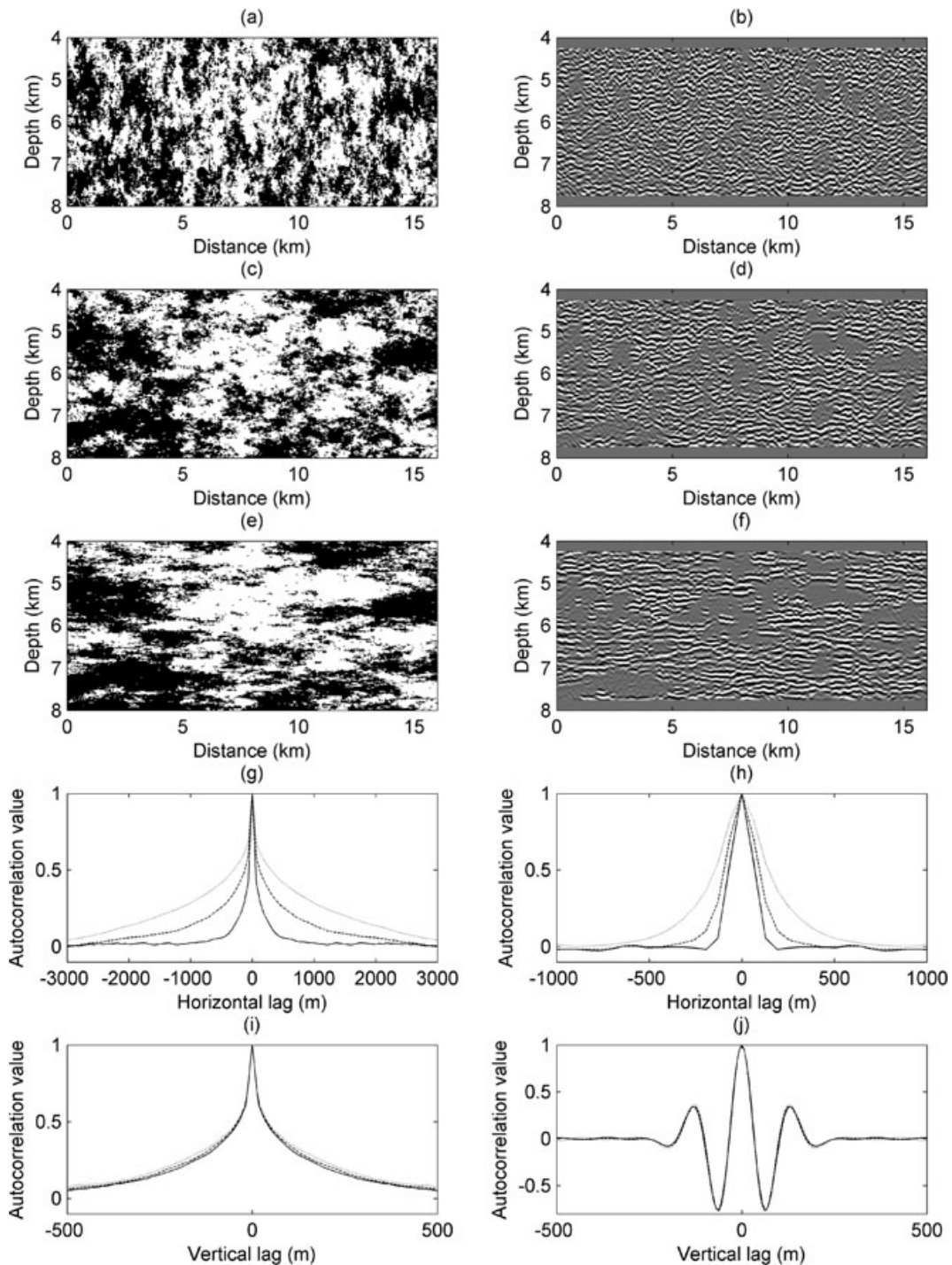


Figure 3. Examination of the effect of varying a_x , holding a_z and ν fixed, on the horizontal and vertical seismic image autocorrelations. See Table 1 for input and best-fitting von Kármán parameter values. (a–f) Bimodal velocity fields and corresponding 15 Hz, zero-offset, finite-difference-based seismic images. (g–h) Corresponding horizontal autocorrelations of the velocity fields and seismic images, respectively. (i–j) Corresponding vertical autocorrelations of the velocity fields and seismic images, respectively. Solid black lines correspond to (a) and (b). Dashed black lines correspond to (c) and (d). Grey lines correspond to (e) and (f).

image, despite keeping a_x approximately constant. Specifically, the lateral correlation length can be seen to shorten as a_z is increased. Considering Fig. 4 we believe that this results because of a change in the aspect ratio of the velocity heterogeneity. The reasons explaining the sensitivity of the lateral correlation structure to only the aspect ratio, and not specifically a_x or a_z when a_x/a_z is held constant, need to be explored in detail in future research efforts. However,

we believe that this phenomenon can be explained heuristically as follows: If we increase a_x but keep a_z fixed, the average length of reflection events in the seismic image will clearly increase and thus we will have an increase in the image’s apparent lateral correlation length. Conversely, if we increase a_z but keep a_x fixed, the average vertical distance between reflectors will increase and consequently there will tend to be less occurrences of reflectors that are in fact

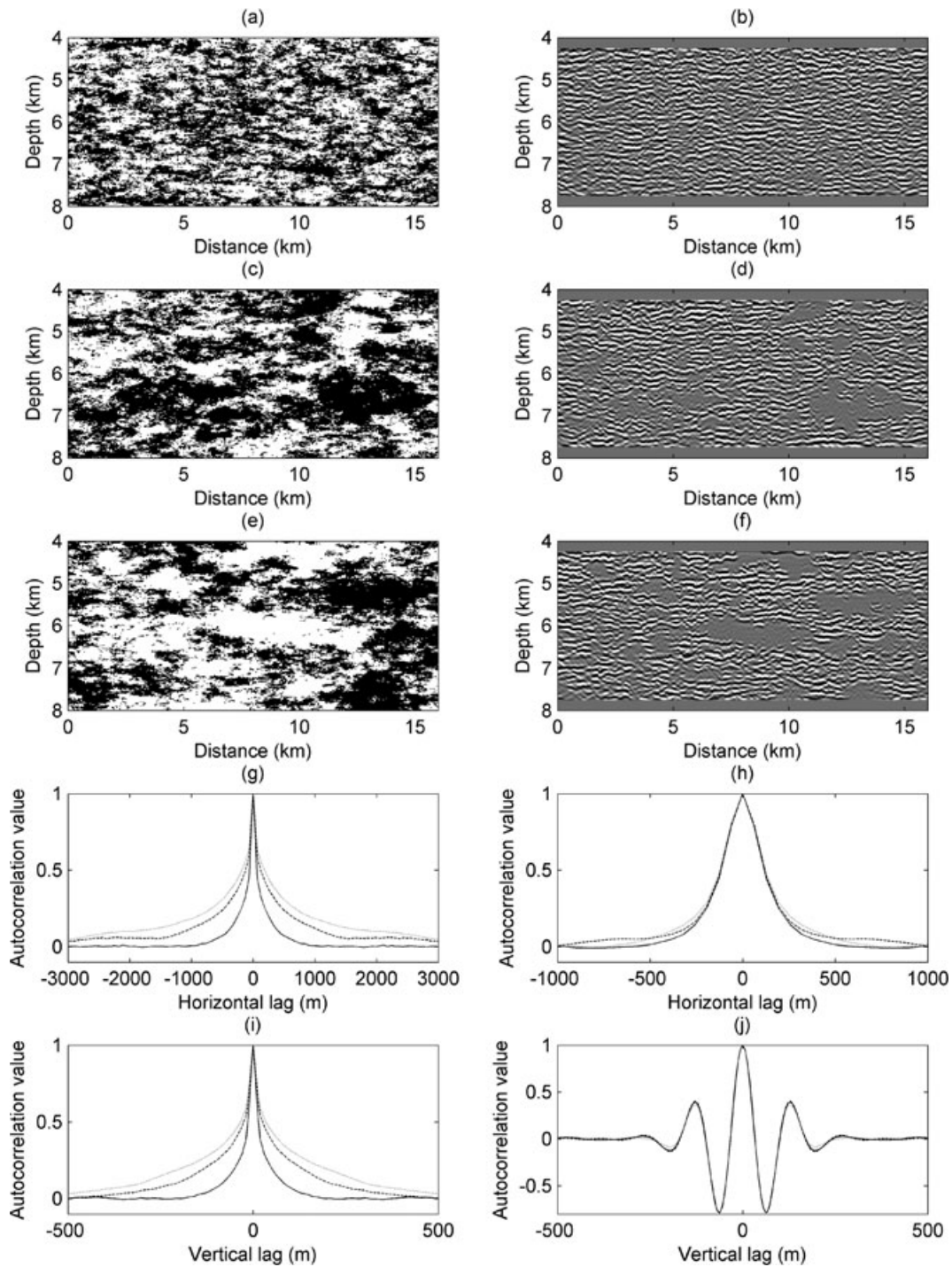


Figure 4. Examination of the effect of varying a_x and a_z , holding the aspect ratio (a_x/a_z) and ν fixed, on the horizontal and vertical seismic image autocorrelations. See Table 1 for input and best-fitting von Kármán parameter values. (a–f) Bimodal velocity fields and corresponding 15 Hz, zero-offset, finite-difference-based seismic images. (g–h) Corresponding horizontal autocorrelations of the velocity fields and seismic images, respectively. (i–j) Corresponding vertical autocorrelations of the velocity fields and seismic images, respectively. Solid black lines correspond to (a) and (b). Dashed black lines correspond to (c) and (d). Grey lines correspond to (e) and (f).

horizontally discontinuous, but effectively ‘line up’ (i.e. are seen as continuous) when convolved with the seismic pulse. This causes a decrease in the apparent correlation length of the seismic image. If a_x and a_z are both increased at the same rate (i.e. the aspect ratio is held constant), the above two effects work against one another resulting in no net effect on the lateral correlation behaviour. In other words, the average length of horizontal reflectors increases, but at

the same time we have less merging of horizontally discontinuous reflection events through convolution with the seismic pulse.

Finally, in Fig. 6, we examine the effects of changing the ν -value of the subsurface velocity heterogeneity while keeping both a_x and a_z approximately constant. The random seed to generate the realizations was also held fixed in this figure to better observe the effect of varying ν on the velocity fields, as well as to isolate its effects on the

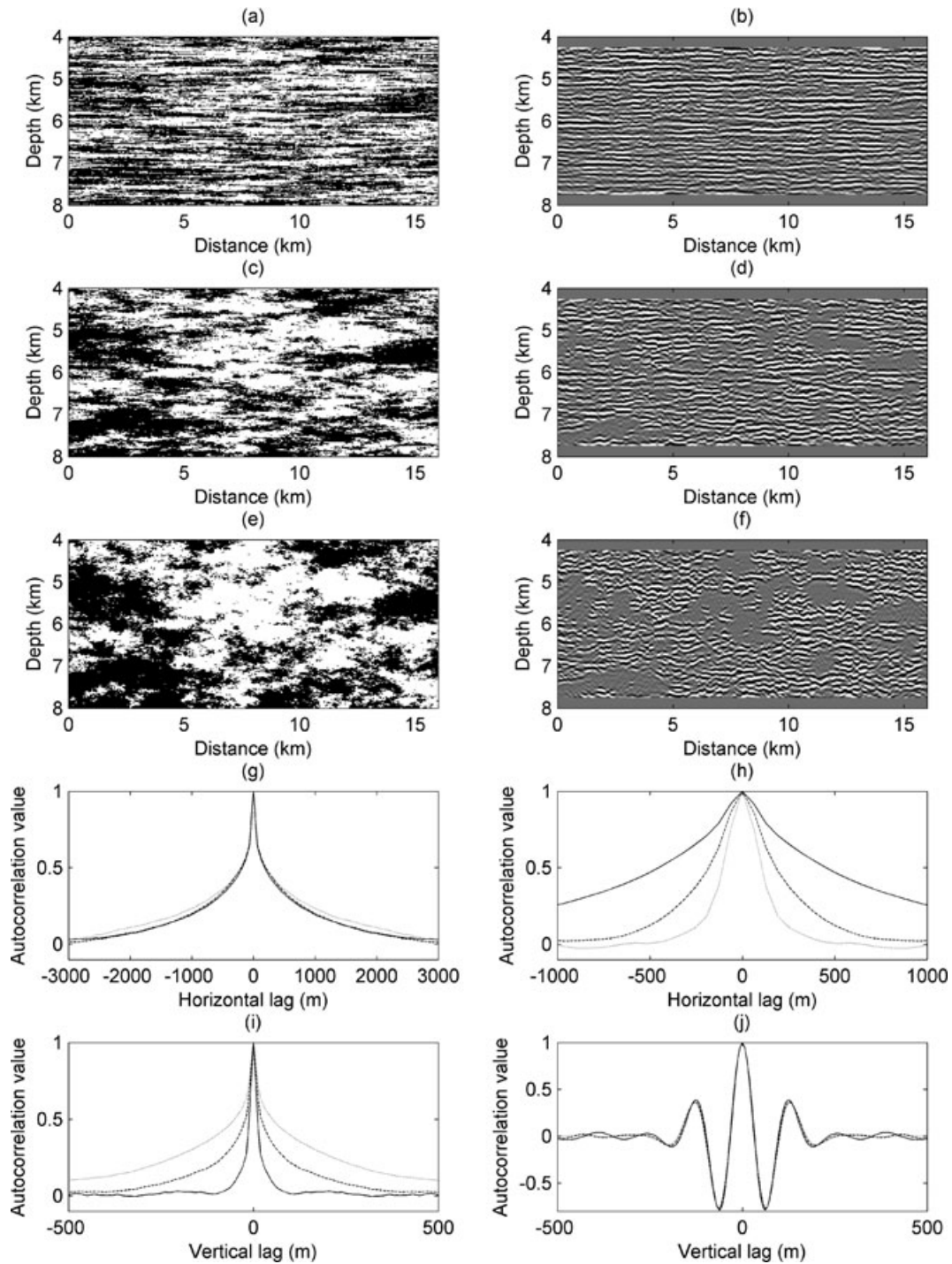


Figure 5. Examination of the effect of varying a_z , holding a_x and ν fixed, on the horizontal and vertical seismic image autocorrelations. See Table 1 for input and best-fitting von Kármán parameter values. (a–f) Bimodal velocity fields and corresponding 15 Hz, zero-offset, finite-difference-based seismic images. (g–h) Corresponding horizontal autocorrelations of the velocity fields and seismic images, respectively. (i–j) Corresponding vertical autocorrelations of the velocity fields and seismic images, respectively. Solid black lines correspond to (a) and (b). Dashed black lines correspond to (c) and (d). Grey lines correspond to (e) and (f).

seismic image from those related to stochastic fluctuations between realizations. After binarization, the ν -values considered are 0.06, 0.15, and 0.47. This selection of values not only essentially covers the range of possible values for bimodal media, but also the range of practically expected values in a broad variety of geological settings (e.g. Holliger & Goff 2003). Note in Figs 6(a), (c), (e) that, as ν is increased, the structure of the velocity heterogeneity becomes con-

siderably less complex, yet because of the constant random seed, the overall pattern of the heterogeneous structure remains the same. As evident from eq. (19), increasing ν increases the slope of the power spectrum and thus decreases the small-scale variability of the medium. The decrease in complexity with increasing ν also clearly translates to the seismic images in Figs 6(b), (d), (f), where we move from a chaotic series of reflections to an image that is

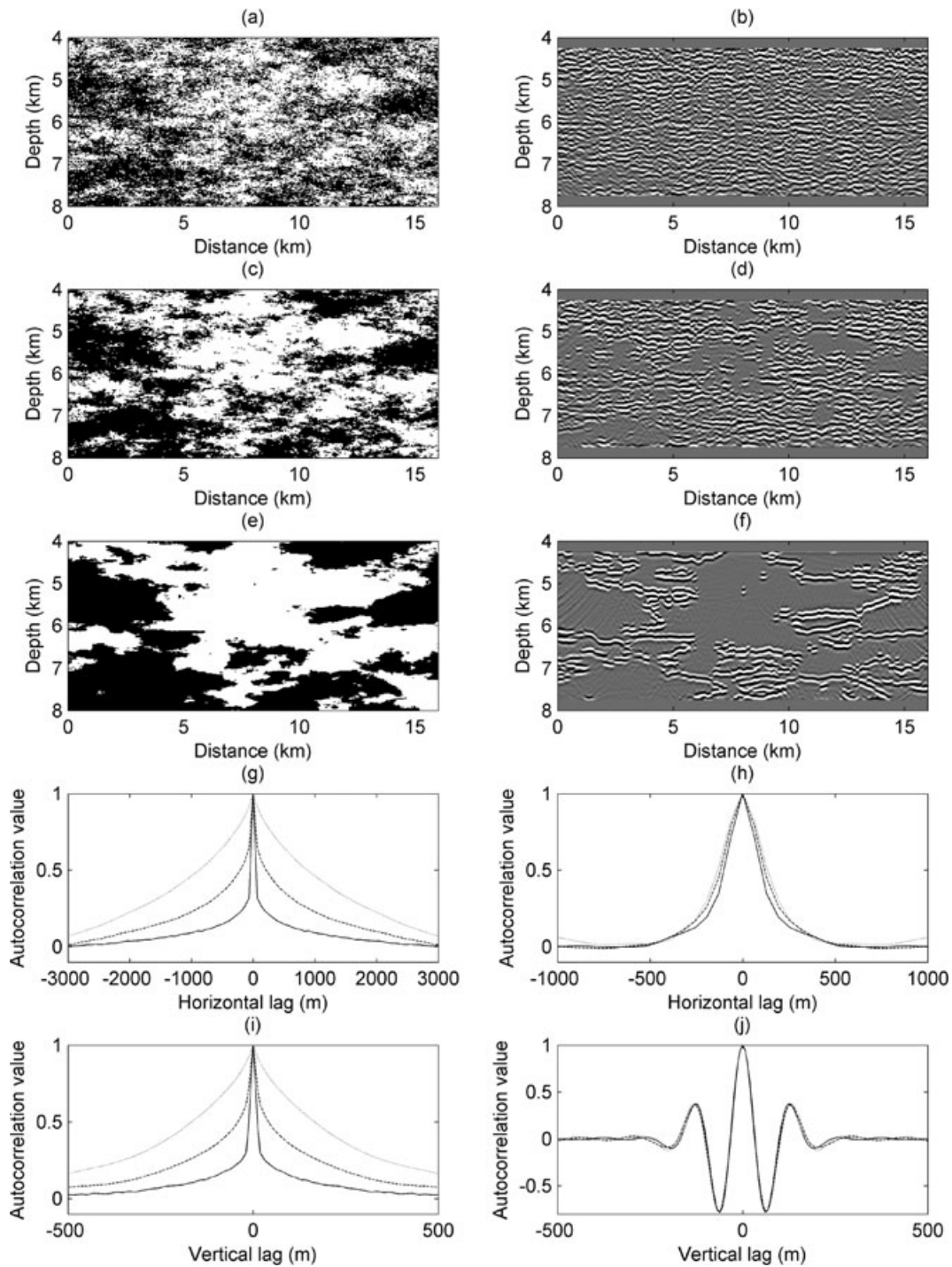


Figure 6. Examination of the effect of varying ν , holding a_x and a_z fixed, on the horizontal and vertical seismic image autocorrelations. See Table 1 for input and best-fitting von Kármán parameter values. (a–f) Bimodal velocity fields and corresponding 15 Hz, zero-offset, finite-difference-based seismic images. (g–h) Corresponding horizontal autocorrelations of the velocity fields and seismic images, respectively. (i–j) Corresponding vertical autocorrelations of the velocity fields and seismic images, respectively. Solid black lines correspond to (a) and (b). Dashed black lines correspond to (c) and (d). Grey lines correspond to (e) and (f).

simple and easy to interpret. Figs 6(g) and (i) show the vertical and horizontal autocorrelations of the velocity fields, respectively. Here, we also see that ν essentially controls the small-scale variability of media and thus the behaviour of the corresponding autocorrelation functions at short lags. Fig. 6(j) demonstrates that the vertical autocorrelation structure in the corresponding seismic images is the same with varying ν . What is again quite surprising, however, is

that, despite the marked changes in the velocity fields and seismic data in Figs 6(a)–(f), the lateral autocorrelations of the images in Fig. 6(h) show little variation. Admittedly, there is a slight increase in the width of the autocorrelation peak of the images as ν increases, but this is subtle and, in our opinion, likely not detectable in a realistic inversion effort. Indeed, given the rather perfect conditions of no noise, zero-offset non-stacked data and only acoustic wave

propagation, we question whether there is any possibility of recovering ν from the second-order statistics of a reflection seismic image. Other tests that we have performed using random fields having different correlation lengths and aspect ratios confirm these observations, which also seem to be consistent with the findings of Carpentier & Roy-Chowdhury (2007) who saw relatively little sensitivity in the estimated lateral ν -value of reflectivity when changing ν in the corresponding velocity fields. In realistic finite-difference-modelled seismic data such as ours, this sensitivity is even further decreased because the wavefield tends to respond only to the macroscopic aspects of the heterogeneity, averaging out the small-scale random fluctuations as a result of non-linear wave propagation effects such as wavefront healing and averaging by the source wavelet (Bean *et al.* 1999; Hurich & Kocurko 2000; Carpentier & Roy-Chowdhury 2007).

Table 2. List of prior parameter ranges for the Monte Carlo inversion, whose results are shown in Figs 7–14.

Figure	Dominant frequency (Hz)	Prior uniform range for a_x (m)	Prior uniform range for a_z (m)	Prior uniform range for ν
7, 8	15	250–350	100–5000	0.1–0.4
9, 10	15	100–1000	100–5000	0.1–0.4
11, 12	27	250–350	100–5000	0.1–0.4
13, 14	27	100–1000	100–5000	0.1–0.4

5 MONTE CARLO INVERSION FOR STOCHASTIC MODEL PARAMETERS

5.1 Methodology

Eq. (16) links the 2-D autocorrelation of a zero-offset seismic reflection image with that of the underlying velocity perturbation field. We saw previously that, when the assumptions used to derive this equation are approximately valid, it allows us to capture the relevant physics of the seismic reflection experiment and effectively predict the stochastic structure of the imaged data. The equation can thus be used to develop an inversion strategy to estimate the correlation properties of the velocity field from those of the seismic image. Given the results of our sensitivity analysis, we expect in advance that such an inversion, when provided with limited prior information, will only allow recovery of the aspect ratio of the velocity heterogeneity and not both the correlation lengths a_x and a_z . We also expect considering Fig. 6 that the inversion will have a limited ability to recover ν . For these reasons, along with the fact that estimating a_x , a_z and ν using eq. (16) is a very non-linear problem, we chose to tackle the inversion stochastically. Stochastic inverse methods are computationally costly and thus generally only allow for the estimation of a small number of model parameters. These methods do, however, naturally account for the existence of multiple solutions, are inherently flexible with regard to how parameter sets are judged as acceptable, and avoid the use of gradient measures on

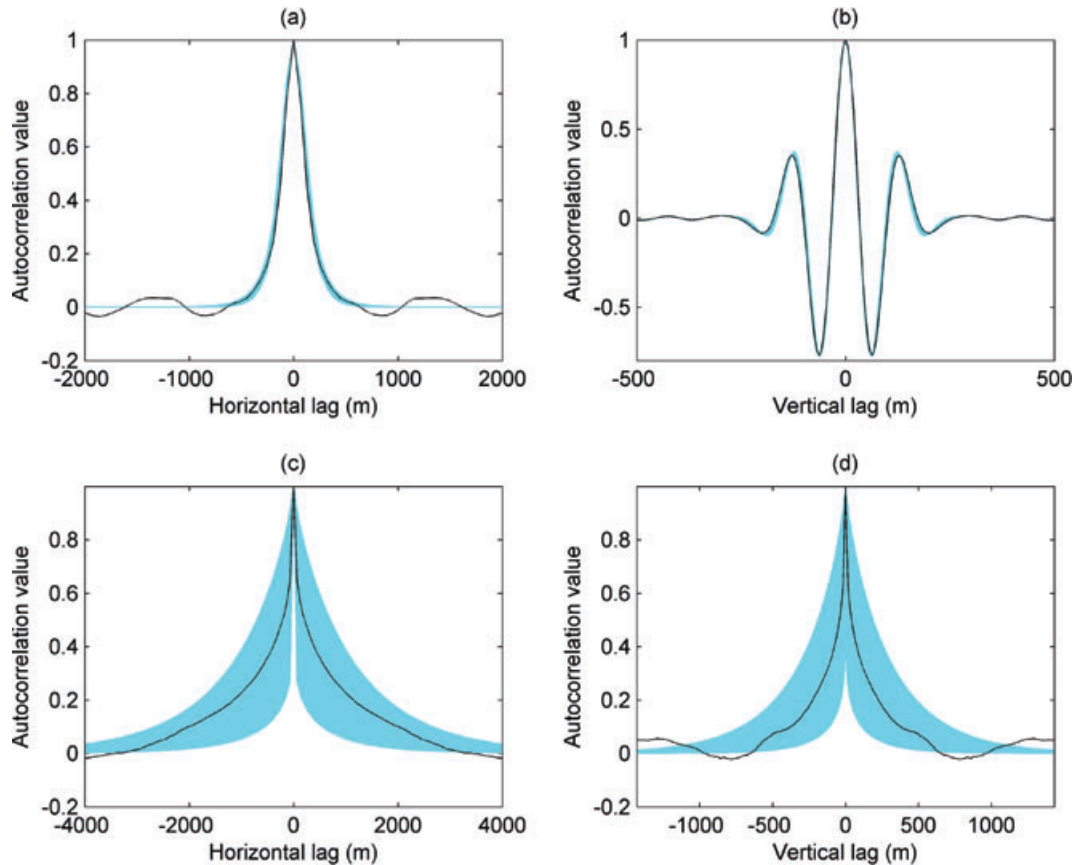


Figure 7. Monte Carlo inversion results for the 15 Hz finite-difference-based seismic image in Fig. 1(c), using a narrow prior range for a_z . See Table 2 for details. (a) and (b) Horizontal and vertical autocorrelations of the seismic image (black), respectively, and the predicted horizontal and vertical image autocorrelations for all of the accepted parameter sets (blue), obtained using eq. (16). (c) and (d) Horizontal and vertical autocorrelations of the true velocity model in Fig. 1(a) (black), respectively, and those corresponding to all of the accepted parameter sets (blue).

a global objective function which is not suitable in the presence of many local minima.

To address the similar problem of estimating the autocorrelation model parameters describing subsurface water content heterogeneity from reflection GPR data, Irving *et al.* (2009) used a Bayesian Markov-chain-Monte-Carlo (McMC) stochastic inversion approach. While Bayesian-McMC methods have the major benefit of embracing formal statistical theory, thus allowing for the determination of valid posterior statistics for the model parameters involved, such posterior uncertainty estimates, in practice, rely upon our having an error-free forward model, or alternatively being able to assess the impact of structural model errors on the observed data, as well as having knowledge of the statistical distribution of the data measurement errors. In our case these conditions are not satisfied. That is, the forward model in eq. (16) relating the velocity and seismic image autocorrelations is only approximate and thus contains difficult-to-quantify structural errors, and we have little knowledge of the nature of the errors in the observed autocorrelation data. For these reasons, we have chosen to perform the stochastic inversion in this paper using a comparatively simple Monte Carlo approach. It is important to note that, although McMC methods can offer significant computational benefits over standard Monte Carlo approaches due to the construction of the Markov chain, in our case the inverse problem only contains three parameters (a_x , a_z and ν) and thus computational expense is not a critical issue. The Monte Carlo inversion strategy that we employ to invert eq. (16) consists of the following steps:

1. Define uniform prior ranges for each of the von Kármán model parameters to be estimated, which describe the 2-D autocorrelation of velocity $R_{vv}(x, z)$.
2. Define criteria for an acceptable fit to the observed lateral autocorrelation of the processed and migrated seismic image, $R_{dd}(x, 0)$. We have found that only fitting in the lateral direction is necessary, as the vertical correlation structure of the seismic image is controlled completely by the source pulse. In other words, if the fit to $R_{dd}(x, 0)$ is adequate, then we will have an adequate fit to the whole 2-D seismic image autocorrelation.
3. Randomly draw a proposed set of values for a_x , a_z and ν from the prior distributions defined in Step 1 and calculate the corresponding $R_{vv}(x, z)$ using eq. (17).
4. Calculate the predicted seismic image autocorrelation, $R_{pp}(x, z)$, using the $R_{vv}(x, z)$ obtained in Step 3 and eq. (16). To determine $R_{ff}(x, z)$ in this equation, we convolve $R_{dd}(0, z)$ with the autocorrelation of a vertical derivative operator and that of the horizontal resolution filter, $h(x)$. As seen in Fig. 2, $R_{dd}(0, z)$ gives a good estimate of the autocorrelation of the input seismic wavelet, $R_{ww}(z)$.
5. Compare the predicted and observed lateral autocorrelations, $R_{pp}(x, 0)$ and $R_{dd}(x, 0)$. If the prediction fits the criteria defined in Step 2, which generally means its lying within upper and lower bounds prescribed around $R_{dd}(x, 0)$, then the proposed set of von Kármán model parameters are considered to be possible given the seismic data and they are accepted. Otherwise, the proposed set of model parameters is rejected.

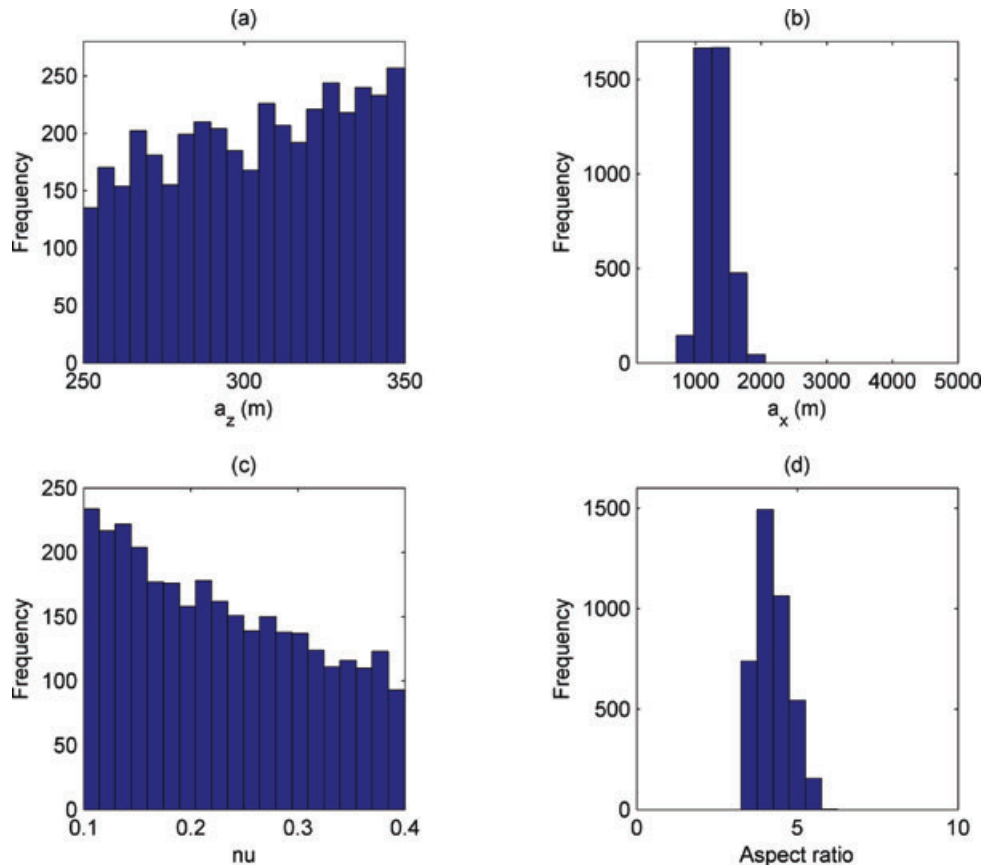


Figure 8. Parameter histograms for the inversion results shown in Fig. 7.

6. Return to Step 3 and repeat until the desired number of accepted realizations for a_x , a_z and ν has been reached.

Specific details regarding the application of the above inversion strategy will be given in the next subsection, where we show the results of inverting the autocorrelations of the 15 and 27 Hz finite-difference-modelled seismic data in Figs 1(d) and (h) for the von Kármán parameters describing the velocity autocorrelation in Fig. 1(b). This is done using two sets of prior information, one where a_z is well constrained and the other where it is not.

5.2 Examples

5.2.1 15 Hz data

We first consider the stochastic inversion of the autocorrelation of the 15 Hz seismic data in Fig. 1(d) when it is assumed that we have reasonably good prior knowledge of the vertical correlation length of the subsurface velocity heterogeneity. In practice, this might come from the analysis of borehole data in the case of the upper crust or when considering near-surface lower and middle crustal analogues. Alternatively, the vertical correlation length could also be estimated using the approach presented by Poppeliers & Levander (2004) and Poppeliers (2007). Knowledge regarding the lateral correlation length and ν -value of the heterogeneity is assumed to be limited. Table 2 shows the prior von Kármán parameter ranges used in this inversion and all of the others to follow, the results of which

are shown in Figs 7 through 14. For this first case, a_z was prescribed a prior uniform distribution having lower and upper bounds of 250 and 350 m, respectively, which rather narrowly bound the true value of 313 m. For a_x , we assumed a broad uniform prior range between 100 and 5000 m, with the true value being equal to 1544 m. For ν , we prescribed a uniform prior range between 0.1 and 0.4, which easily captures all possible values for this parameter in crustal rocks (e.g. Holliger & Goff 2003), the true value being equal to 0.15.

To carry out the inversion procedure described in Section 5.1, we require some measure of what represents an acceptable fit of the predicted lateral autocorrelation data, $R_{pp}(x, 0)$, to the observed lateral autocorrelation of the seismic image, $R_{dd}(x, 0)$. For all of the inversions presented in this paper, we defined this fit by setting bounds around $R_{dd}(x, 0)$ within which acceptable $R_{pp}(x, 0)$ curves must lie. We have found that the best results are obtained when such bounds are specified along both the horizontal and vertical axes. In other words, a predicted $R_{pp}(x, 0)$ curve is deemed acceptable if, at each point on the curve, it lies either vertically or horizontally within a prescribed distance from the observed $R_{dd}(x, 0)$ curve. In our case, lying either within 25 m of the observed curve along the horizontal lag axis, or within 0.03 units of the observed curve along the autocorrelation value axis, meant that a predicted curve could be accepted (Fig. 7). Our choice of the bounding values is rather subjective, but the general idea is that they should best reflect our belief about the maximum distance that acceptable autocorrelation curves can stray from the observed curve. Although not without problems, this choice is far less difficult than the one that must be made in

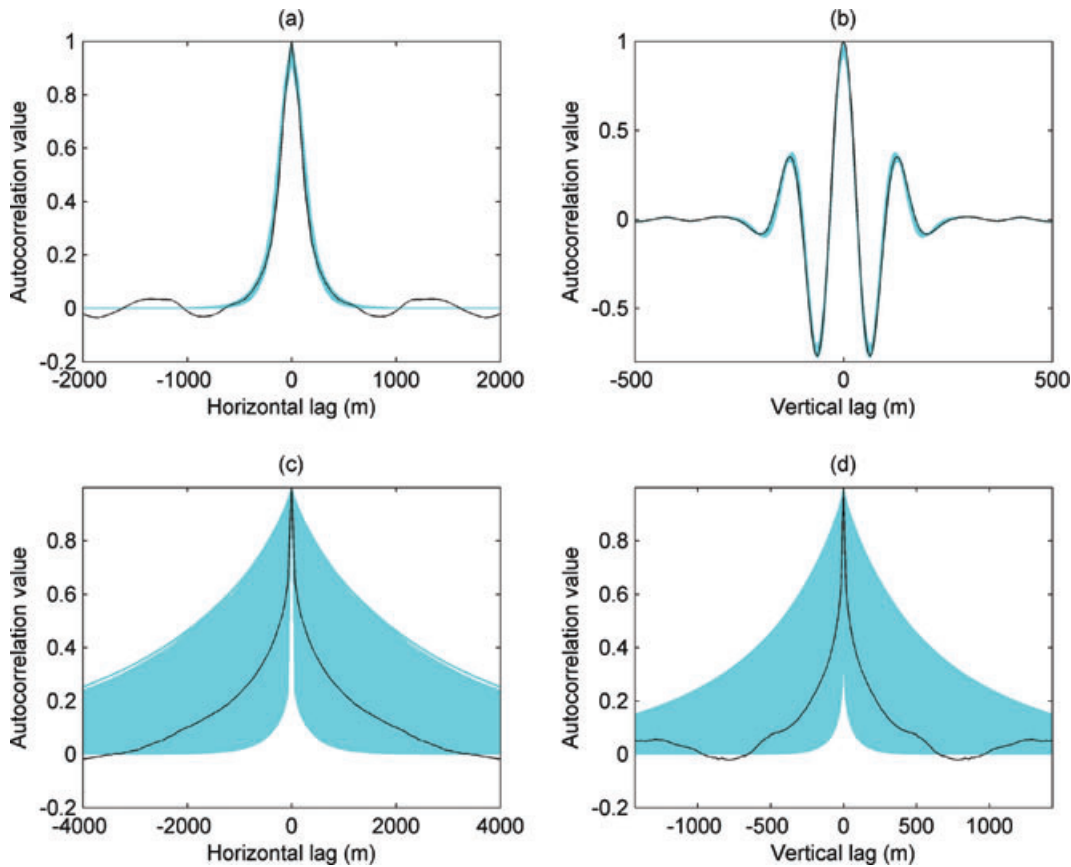


Figure 9. Monte Carlo inversion results for the 15 Hz finite-difference-based seismic image in Fig. 1(c), using a broad prior range for a_z . See Table 2 for details. (a) and (b) Horizontal and vertical autocorrelations of the seismic image (black), respectively, and the predicted horizontal and vertical image autocorrelations for all of the accepted parameter sets (blue), obtained using eq. (16). (c) and (d) Horizontal and vertical autocorrelations of the true velocity model in Fig. 1(a) (black), respectively, and those corresponding to all of the accepted parameter sets (blue).

the corresponding MCMC inversion approach, where the statistical distribution of the errors in the seismic data autocorrelation must be specified (e.g. Irving *et al.* 2009). It is important to note that, in our examples, we only evaluate the fit of $R_{pp}(x, 0)$ to $R_{dd}(x, 0)$ at lag values between -1000 and 1000 m. This range captures the key behaviour of the lateral autocorrelations of both the 15 and 27 Hz seismic data (Fig. 1) and thus considering the fit at greater lags is not necessary.

The Monte Carlo inversion algorithm was run until 4000 realizations for a_x , a_z and ν were accepted. On the same 3.16 GHz computer with 3.23 GB of RAM used to perform the seismic modelling, this took approximately 20 hr. Figs 7 and 8 show the results obtained for the first inversion, again where relatively good knowledge regarding a_z was assumed. In Fig. 7(a), the observed lateral seismic data autocorrelation is plotted in black, whereas all 4000 predicted autocorrelations that were accepted are plotted in blue. Note that all of the accepted curves match closely the observed curve because of the fitting constraints imposed along both axes described above. Fig. 7(b), on the other hand, shows the observed and predicted vertical seismic data autocorrelations. Here, we see that, despite our not imposing any fitting constraints in the vertical direction in the inversion procedure, all accepted sets of model parameters allow us to also match $R_{dd}(0, z)$ accurately. This again is because the vertical correlation structure of the seismic data is controlled by the seismic wavelet and it confirms that evaluating data fit only in the horizontal direction is sufficient to match the whole 2-D seismic data autocorrelation. Finally, Figs 7(c) and (d) show the lateral and vertical autocorrelations of velocity corresponding to all 4000 accepted sets of von Kármán model parameters, respectively,

along with the corresponding ‘true’ curves for the velocity field in Fig. 1(a). Although the accepted parameter sets predict a close match to the observed autocorrelations of the seismic data, note that they represent a significantly broader spread about the true velocity field autocorrelations. This is a result of the non-uniqueness of the inverse problem, in the sense that there are a number of velocity autocorrelations and corresponding von Kármán parameterizations that are able to well explain the second-order statistics of the seismic data. Nevertheless, the predicted curves in Figs 7(c) and (d) are still reasonably well constrained about the true curves.

In Fig. 8, we show the marginal histograms for a_z , a_x , ν and a_x/a_z that were computed from the 4000 parameter sets obtained in the inversion procedure. Fig. 8(a) shows that the inversion of the seismic image autocorrelation data does not allow for any further refinement in our knowledge about the vertical correlation length of velocity. Based on the results of our sensitivity analysis, this is expected because the prior range for a_x was set to be broad and any velocity models having the correct aspect ratio should predict reasonably well the seismic image autocorrelation. That is, for each a_z value within the narrow prior range from 250 to 350 m, we expect there to be an a_x value that allows a good prediction of $R_{dd}(x, 0)$. Conversely, in Fig. 8(b), we see that the inversion has done a good job of significantly narrowing our uncertainty regarding the horizontal correlation length, which was prescribed *a priori* to lie between 100 and 5000 m. Here, the output histogram for a_x has a distinctly normal appearance, with the mean and standard deviation being equal to 1285 m and 195 m, respectively. This agrees quite well with the true value of 1544 m and confirms that, for the case where a_z is assumed to be relatively well known and a restricted prior range is provided

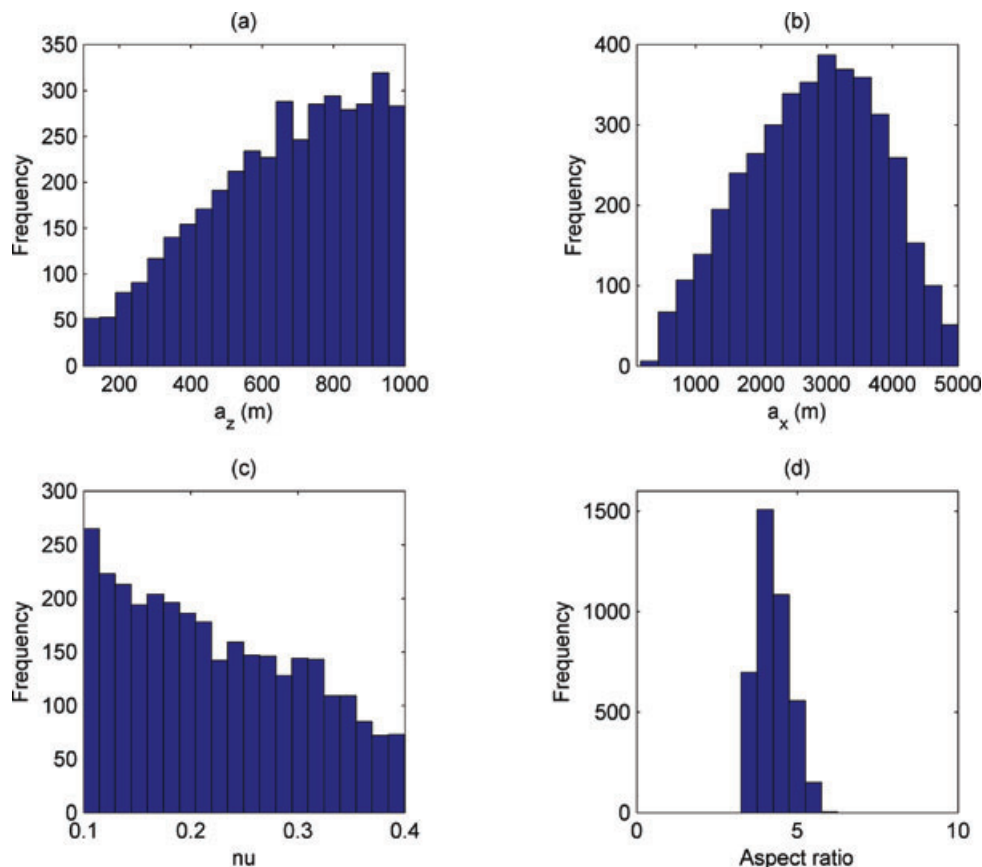


Figure 10. Parameter histograms for the inversion results shown in Fig. 9.

for this parameter, we can successfully recover a_x from the second-order statistics of the seismic data. Fig. 8(c) demonstrates that, as expected, the inversion procedure has little success in recovering the ν -value of the velocity heterogeneity. Values at the lower end of the prior range between 0.1 and 0.4 can be seen to be preferred, but an identification of ν from the mean of the output realizations is not possible. Finally, we see in Fig. 8(d) that, similar to the horizontal correlation length, the aspect ratio of the velocity heterogeneity is well recovered. The output mean and standard deviation of a_x/a_z are 4.24 and 0.52, which are in reasonably good agreement with the true value of 4.93.

We now investigate again the inversion of the 15 Hz autocorrelation data in Fig. 1(d), but for the case where limited information is assumed regarding the vertical correlation length of velocity. All of the inversion parameters were kept the same as before except the prior range for a_z , which was now set to have lower and upper bounds of 100 and 1000 m, respectively (Table 2). Figs 9 and 10 show the results. In Figs 9(a) and (b), we see again that all accepted sets of von Kármán model parameters provide a close fit to both the horizontal and vertical seismic data autocorrelations, despite the fitting being enforced only in the horizontal direction at lags between -1000 and 1000 m. In Figs 9(c) and (d), we also observe again that the accepted parameter sets translate into a considerable spread of velocity model autocorrelations about the true curves. In this case, however, note that the spread of these models is much larger than in the case where a_z was well constrained. Since we have sensitivity

to only the aspect ratio of the velocity heterogeneity and both a_x and a_z were prescribed broad uniform prior distributions, there is a wide range of a_x - a_z combinations that allow adequate fitting of the image autocorrelation data. Looking at the output histograms, Fig. 10(a) shows that, because of this non-uniqueness, the inversion procedure essentially provides no useful information regarding the true value of a_z . In fact, larger values in the considered interval can be seen to be preferred, despite the true value being only 313 m. Regarding a_x , we also see that the inversion provides unreliable results. Although Fig. 10(b) shows a peaked distribution with a distinctly normal appearance, the calculated mean and standard deviation of this distribution are 2794 m and 1024 m, which are not very helpful considering that the true value is 1544 m. With respect to the aspect ratio of the velocity heterogeneity, however, we see in Fig. 10(d) that the inversion is again successful, yielding a peaked distribution with a mean and standard deviation of 4.24 and 0.50, respectively. We can therefore conclude that, despite our inability to accurately reduce our uncertainty regarding a_z and a_x for the case where little prior information is provided about these parameters, we can still well recover the structural aspect ratio a_x/a_z . Given increasing evidence that much of the Earth's crustal seismic structure is likely to be scale-invariant in nature and characterized by a relatively narrow range of small ν -values (Holliger & Goff 2003), it can indeed be argued that the aspect ratio represents the most valuable and important parameter in terms of the second-order spatial statistics. Note that in Fig. 10(c) we again have little refinement in our knowledge

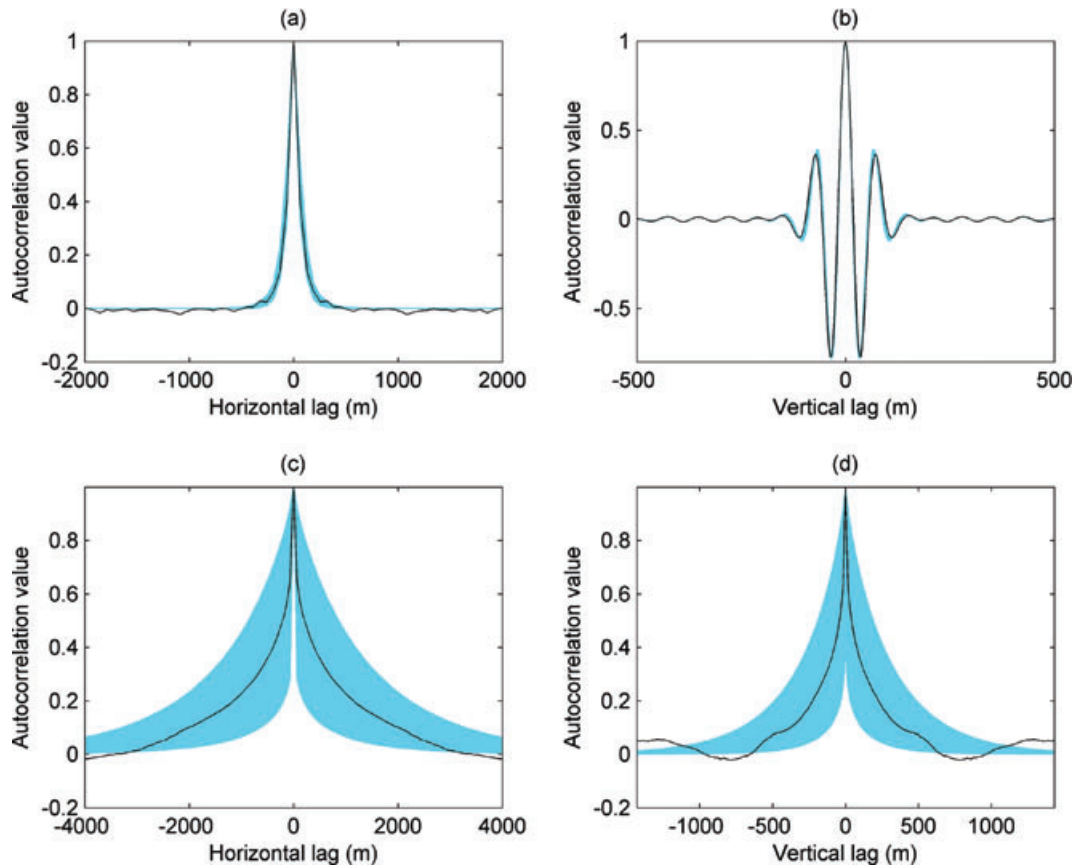


Figure 11. Monte Carlo inversion results for the 27 Hz finite-difference-based seismic image in Fig. 1(g), using a narrow prior range for a_z . See Table 2 for details. (a) and (b) Horizontal and vertical autocorrelations of the seismic image (black), respectively, and the predicted horizontal and vertical autocorrelations for all of the accepted parameter sets (blue), obtained using eq. (16). (c) and (d) Horizontal and vertical autocorrelations of the true velocity model in Fig. 1(a) (black), respectively, and those corresponding to all of the accepted parameter sets (blue).

of ν through the inversion, with values near the lower end of the prescribed prior range being slightly preferred.

Finally, we also wish to point out that these empirical results are consistent with the findings of a recent analytical sensitivity analysis carried out in the power spectral domain (Irving & Holliger 2010). The results of this analytical study confirm that surface-based seismic and GPR reflection images are essentially insensitive to the individual values of the horizontal and vertical correlation lengths of the subsurface velocity fluctuations, a_x and a_z , but exhibit a high sensitivity to the corresponding structural aspect ratio, a_x/a_z . Conversely, these analytical results indicate that surface-based reflection images should have a somewhat higher sensitivity to the ν -value than we observe in this numerical study. This may again point to the fact that, while the PRS model is in general a very good approximation of a final seismic or GPR reflection image, there are some effects of dynamic wave propagation and/or data acquisition and processing which are not accounted for.

5.2.2 27 Hz data

In an identical manner as for the 15 Hz data discussed above, we next explore the inversion of the autocorrelation of the 27 Hz seismic data in Fig. 1(h). The goal here is to evaluate how well the inversion procedure performs with different frequency data corresponding to the same underlying crustal velocity field. Figs 11 and 12 show the results obtained for the case where narrow and broad prior ranges were prescribed for a_z and a_x , respectively, whereas Figs 13 and 14 show the results when, as before, both a_x and a_z were given broad

uniform prior bounds (Table 2). Note that Figs 11–14 are similar in character to Figs 7–10, which illustrates that changing the frequency of the seismic experiment does not change the fundamental validity of our previous conclusions. In the case where a_z was well constrained, the inversion provides a good estimate of a_x and the aspect ratio, with the mean and standard deviation of the former being equal to 1454 m and 285 m and those of the latter being equal to 4.80 and 0.82, respectively. In the case where a_z and a_x were prescribed to be uncertain, on the other hand, only the aspect ratio is well recovered, in this case having an output mean and standard deviation of 4.74 and 0.77. One item of particular interest in Figs 12 and 14, which is somewhat counter-intuitive, is the increased standard deviation of the estimates of a_x and a_x/a_z compared to the lower frequency results in Figs 8 and 10. Intuitively, one might expect that the higher-frequency data, which provide a higher resolution seismic image of the subsurface heterogeneity, would yield a more precise estimate of the von Kármán model parameters for the crustal velocity field. However, this is not the case and we believe results from the fact that the lateral correlation statistics of the higher frequency seismic image are actually less sensitive to changes in the velocity correlation model parameters.

6 CONCLUSIONS

We have presented in this paper a simple conceptual model, based on the PRS formulation, that allows us to quantitatively link the 2-D autocorrelation of a properly processed and depth-migrated seismic image with that of the underlying crustal velocity distribution. This

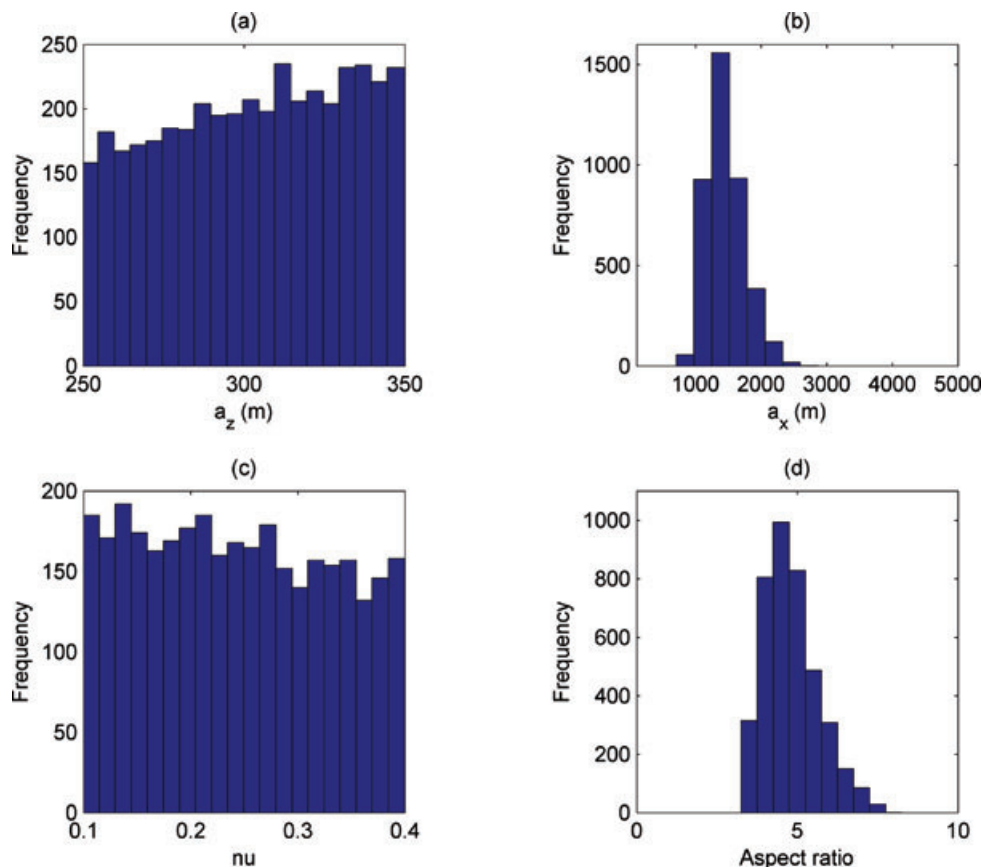


Figure 12. Parameter histograms for the inversion results shown in Fig. 11.

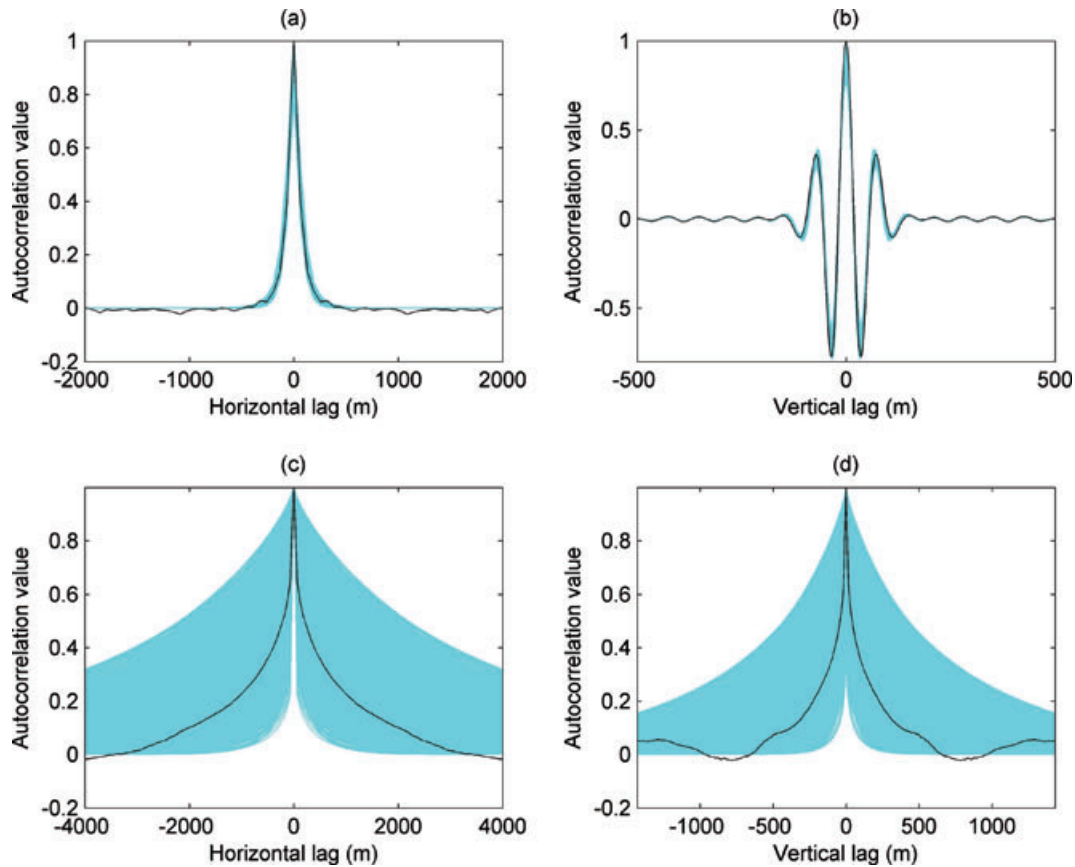


Figure 13. Monte Carlo inversion results for the 27 Hz finite-difference-based seismic image in Fig. 1(g), using a broad prior range for a_z . See Table 2 for details. (a) and (b) Horizontal and vertical autocorrelations of the seismic image (black), respectively, and the predicted horizontal and vertical image autocorrelations for all of the accepted parameter sets (blue), obtained using eq. (16). (c) and (d) Horizontal and vertical autocorrelations of the true velocity model in Fig. 1a (black), respectively, and those corresponding to all of the accepted parameter sets (blue).

model is valid for the case of single scattering in the subsurface and when the effects of dispersion and mode conversions in the data are minor or have been removed by processing. Unlike previous theoretical efforts, our formulation correctly predicts the often-large changes in the lateral autocorrelation of a seismic image caused by vertical filtering operations on the velocity field, and is thus well suited for an inversion strategy to estimate the stochastic parameters describing the correlation structure of velocity from the second-order statistics of the image.

In a simple sensitivity study, we found that the lateral autocorrelation of a seismic image is strongly affected by changes in the aspect ratio of the underlying crustal velocity heterogeneity, but shows little dependence on the vertical or horizontal correlation lengths individually when the aspect ratio remains unchanged. This interesting result will be explored in detail in a future publication. A small amount of sensitivity was also seen to the ν -value of the heterogeneity, but in our experience not enough to be detectable through any inversion effort. The vertical autocorrelation of a seismic image, on the other hand, was demonstrated to be only sensitive to the second-order statistics of the seismic source wavelet. This result is expected as it forms the basis for standard stochastic deconvolution algorithms, yet it is critically important as it provides us with an effective means of estimating $R_{ww}(z)$ and thus $R_{ff}(x, z)$, which is required to use our model in the corresponding inversion.

Results of testing a Monte Carlo inversion methodology based on our model confirmed that, without prior knowledge of either the

vertical or horizontal correlation lengths of the subsurface velocity field, the inverse problem is inherently non-unique in that multiple combinations of a_x and a_z will allow for adequate prediction of the 2-D autocorrelation of a seismic image. All of these acceptable combinations, however, correspond to approximately the correct aspect ratio of the velocity heterogeneity, which shows that a_x/a_z is a quantity that we have the potential to recover in any case. We also found that varying the dominant frequency of the seismic data by almost a factor of two did not impact these findings.

It is important to emphasize that the work presented in this paper should not be viewed as a complete solution to the problem of estimating the correlation properties of crustal velocity heterogeneity from seismic reflection data, but rather as a feasibility study investigating, under optimal conditions, just what we might hope to recover regarding a_x , a_z and ν from the second-order statistics of a seismic image. Compared to previous work, this research represents a significant step forward in that it correctly accounts for a number of key features in the production of a seismic image that were erroneously dealt with in the past, namely the vertical differentiation of velocity to obtain reflection coefficients and convolution with the source wavelet.

Note that a number of critical assumptions were made to allow the evaluation of our methodology under a best-case scenario. These assumptions must be dealt with in future work to evaluate the potential of the methodology in a field setting. In particular, we must now investigate the effectiveness of the inversion strategy in the presence

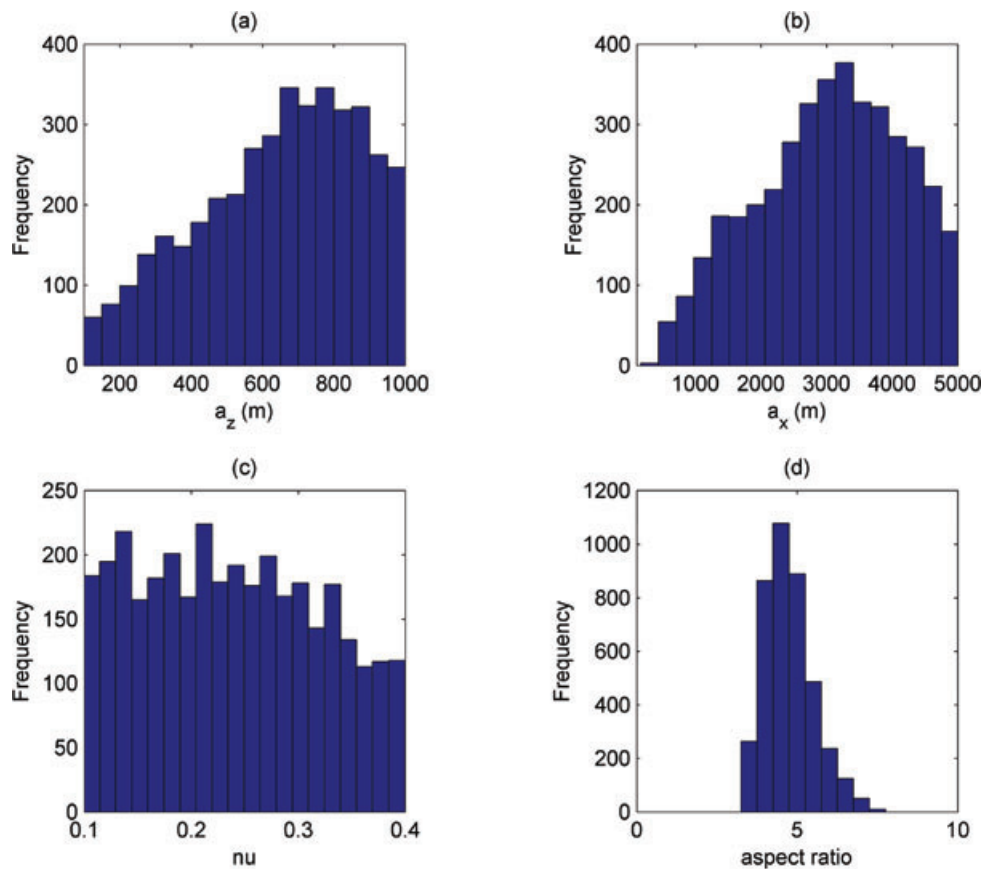


Figure 14. Parameter histograms for the inversion results shown in Fig. 13.

of noise, under elastic wave propagation, and using CMP-stacked seismic reflection data having finite aperture. Preliminary results on more realistic data sets indicate that strategy has much potential.

ACKNOWLEDGMENTS

This research was supported by a grant from the Swiss National Science Foundation. Comments and suggestions by Richard Hobbs, an anonymous referee as well as by the editor David Halliday were constructive and insightful and helped to improve the quality of this manuscript. We wish to thank Johan Robertsson for the permission to use his seismic modelling code.

REFERENCES

- Bean, C., Marsan, D. & Martini, F., 1999. Statistical measures of crustal heterogeneity from reflection seismic data: the role of seismic bandwidth, *Geophys. Res. Lett.*, **26**, 3241–3244.
- Berkhout, A., 1984. *Seismic Resolution: A Quantitative Analysis of Resolving Power of Acoustical Echo Techniques*, Geophysical Press, London.
- Carpentier, S. & Roy-Chowdhury, K., 2007. Underestimation of scale lengths in stochastic fields and their seismic response: a quantification exercise, *J. geophys. Int.*, **169**, 547–562.
- Chen, J. & Schuster, G., 1999. Resolution limits of migrated images, *Geophysics*, **64**, 1046–1053.
- Claerbout, J., 1985. *Imaging the Earth's Interior*, Blackwell Scientific Publications, Oxford.
- Dolan, S., Bean, C. & Riollet, B., 1998. The broad-band fractal nature of heterogeneity in the upper crust from petrophysical logs, *J. geophys. Int.*, **132**, 489–507.

- Frankel, A. & Clayton, R., 1986. Finite difference simulations of seismic scattering Implications for the propagation of short-period seismic waves in the crust and models of crustal heterogeneity, *J. geophys. Res.*, **91**, 6465–6489.
- Gibson, B., 1991. Analysis of lateral coherency in wide-angle seismic images of heterogeneous targets, *J. geophys. Res.*, **96**, 10 261–10 273.
- Gibson, B. & Levander, A., 1988. Lower crustal reflectivity patterns in wide-angle seismic recordings, *Geophys. Res. Lett.*, **15**, 617–620.
- Gibson, B. & Levander, A., 1990. Apparent layering in common-midpoint stacked images of two-dimensionally heterogeneous targets, *Geophysics*, **55**, 1466–1477.
- Goff, J. & Jordan, T., 1988. Stochastic modeling of seafloor morphology: inversion of sea beam data for second-order statistics, *J. Geophys. Res. - Solid Earth*, **93**, 13 589–13 608.
- Goff, J. & Levander, A., 1996. Incorporating ‘sinuous connectivity’ into stochastic models of crustal heterogeneity: examples from the Lewisian gneiss complex, Scotland, the Franciscan formation, California, and the Hafafit gneiss complex, Egypt, *J. geophys. Res.*, **101**, 8489–8502.
- Goff, J., Holliger, K. & Levander, A., 1994. Modal fields: a new method for characterization of random seismic velocity heterogeneity, *Geophys. Res. Lett.*, **21**, 493–496.
- Goovaerts, P., 1997. *Geostatistics for Natural Resources Evaluation*, Oxford University Press, New York.
- Hestholm, S., Husebye, E. & Ruud, B., 1994. Seismic wave propagation in complex crust-upper mantle media using 2-D finite-difference synthetics, *J. geophys. Int.*, **118**, 643–670.
- Holliger, K., 1996. Upper-crustal seismic velocity heterogeneity as derived from a variety of P-wave sonic logs, *J. geophys. Int.*, **125**, 813–829.
- Holliger, K., 1997. Seismic scattering in the upper crystalline crust based on evidence from sonic logs, *J. geophys. Int.*, **128**, 65–72.

- Holliger, K. & Goff, J., 2003. A generalized model for the 1/f-scaling nature of seismic velocity fluctuations, in *Heterogeneity in the Crust and Upper Mantle: Nature, Scaling, and Seismic Properties*, pp. 131–154, eds Goff, J. & Holliger, K., Kluwer Academic/Plenum Scientific Publishers, New York.
- Holliger, K. & Levander, A., 1992. A stochastic view of lower crustal fabric based on evidence from the Ivrea Zone, *Geophys. Res. Lett.*, **19**, 1153–1156.
- Holliger, K. & Levander, A., 1994. Seismic structure of gneissic/granitic upper crust: geological and petrophysical evidence from the Strona-Ceneri Zone (northern Italy) and implications for crustal seismic exploration, *J. geophys. Int.*, **119**, 497–510.
- Holliger, K., Carbonell, R. & Levander, A., 1992. Sensitivity of the lateral correlation function in deep seismic reflection data, *Geophys. Res. Lett.*, **19**, 2263–2266.
- Holliger, K., Levander, A. & Goff, J., 1993. Stochastic modeling of the reflective lower crust-Petrophysical and geological evidence from the Ivrea Zone (northern Italy), *J. geophys. Res.*, **98**, 11 967–11 980.
- Holliger, K., Levander, A., Carbonell, R. & Hobbs, R., 1994. Some attributes of wavefields scattered from Ivrea-type lower crust, *Tectonophysics*, **232**, 267–279.
- Hurich, C., 1996. Statistical description of seismic reflection wavefields: a step towards quantitative interpretation of deep seismic reflection profiles, *J. geophys. Int.*, **125**, 719–728.
- Hurich, C. & Kocurko, A., 2000. Statistical approaches to interpretation of seismic reflection data, *Tectonophysics*, **329**, 251–267.
- Hurich, C. & Smithson, S., 1987. Compositional variation and the origin of deep crustal reflections, *Earth planet. Sci. Lett.*, **85**, 416–426.
- Irving, J., & Holliger, K., 2010. Geostatistical inversion of seismic and Ground-Penetrating Radar reflection images: what can we actually resolve? *Geophys. Res. Lett.*, in press, doi:10.1029/2010GL044852.
- Irving, J., Holliger, K. & Knight, R., 2009. Estimation of the lateral correlation structure of subsurface water content from surface-based ground-penetrating radar reflection images, *Water Resour. Res.*, **45**, W09407, doi:09410.01029/02008WR007646.
- Larkin, S., Levander, A., Okaya, D. & Goff, J., 1996. A deterministic and stochastic velocity model for the Salton Trough/Basin and Range transition zone and constraints on magmatism during rifting, *J. geophys. Res.*, **101**, 27 883–27 897.
- Leary, P., 1991. Deep borehole log evidence for fractal distribution of fractures in crystalline rock, *J. geophys. Int.*, **107**, 615–627.
- Levander, A., England, R., Smith, S., Hobbs, R., Goff, J. & Holliger, K., 1994a. Stochastic characterization and seismic response of upper and middle crustal rocks based on the Lewisian gneiss complex, Scotland, *J. geophys. Int.*, **119**, 243–259.
- Levander, A., Hobbs, R., Smith, S., England, R., Snyder, D. & Holliger, K., 1994b. The crust as a heterogeneous ‘optical’ medium, or ‘crocodiles in the mist’, *Tectonophysics*, **232**, 281–297.
- Line, C., Hobbs, R. & Snyder, D., 1998. Estimates of upper-crustal heterogeneity in the Baltic Shield from seismic scattering and borehole logs, *Tectonophysics*, **286**, 171–183.
- Poppeliers, C., 2007. Estimating vertical stochastic scale parameters from seismic reflection data: deconvolution with non-white reflectivity, *J. geophys. Int.*, **168**, 769–778.
- Poppeliers, C. & Levander, A., 2004. Estimation of vertical stochastic scale parameters in the Earth’s crystalline crust from seismic reflection data, *Geophys. Res. Lett.*, **31**, L13607, doi:10.1029/2004GL019538.
- Pullammanappallil, S., Levander, A. & Larkin, S., 1997. Estimation of crustal stochastic parameters from seismic exploration data, *J. geophys. Res.*, **102**, 15 269–15 286.
- Robertsson, J., Blanch, J. & Symes, W., 1994. Viscoelastic finite difference modeling, *Geophysics*, **59**, 1444–1456.
- Roth, M. & Korn, M., 1993. Single scattering theory versus numerical modelling in 2-D random media, *Geophys. J. Int.*, **112**, 124–140.
- Stolt, R., 1978. Migration by Fourier transform, *Geophysics*, **43**, 23–48.
- Stolt, R. & Benson, A., 1986. *Seismic Migration*, Geophysical Press, London.
- Ulrych, T., 1999. The whiteness hypothesis: reflectivity, inversion, chaos, and Enders, *Geophysics*, **64**, 1512–1523.
- Wu, R. & Aki, K., 1985. The fractal nature of the inhomogeneities in the lithosphere evidenced from seismic wave scattering, *Pure appl. Geophys.*, **123**, 805–818.
- Wu, R., Xu, Z. & Li, X., 1994. Heterogeneity spectrum and scale-anisotropy in the upper crust revealed by the German continental deep-drilling (KTB) holes, *Geophys. Res. Lett.*, **21**, 911–914.
- Yilmaz, Ö., 1987. *Seismic Data Processing*, Society of Exploration Geophysicists, Tulsa.